

Communication Modes with Large Intelligent Surfaces in the Near Field

Nicoló Decarli, *Member, IEEE*, Davide Dardari, *Senior Member, IEEE*

Abstract

This paper proposes a practical method for the definition of multiple communication modes when antennas operate in the near-field region, by realizing ad-hoc beams exploiting the focusing capability of large antennas. The beamspace modeling proposed to define the communication modes is then exploited to derive expressions for the number of communication modes (i.e., degrees of freedom) in a generic setup, beyond the traditional paraxial approximation, together with closed-form definitions for the basis set at the transmitting and receiving antennas for several cases of interest, such as for the communication between a large antenna and a small antenna. Numerical results indicate that quasi-optimal communication can be obtained starting from focusing functions. This translates into the possibility of a significant enhancement of the channel capacity even in line-of-sight channel condition without the need of resorting to optimal but complex phase/amplitude antenna profiles as well as intensive numerical simulations. Traditional results valid under paraxial approximation are revised in light of the proposed modeling, showing that similar conclusions can be obtained from different perspectives.

Index Terms

Holographic MIMO, communication modes, fundamental limits, degrees of freedom, beamspace, large intelligent surfaces, near field.

I. INTRODUCTION

The even-increasing demand for high-speed wireless communication is requiring a shift towards high frequency (e.g., millimeter-wave and terahertz) where large bandwidth is available [1], [2]. In this context, the introduction of new technologies such as intelligent surfaces made of metamaterials has been proposed to realize passive intelligent reflecting surfaces (IRSs) and active large intelligent surfaces (LISs) used as highly-flexible antennas [3]–[9]. In fact, metamaterials enable the manipulation of the electromagnetic (EM) field or the local control of amplitude and phase reflecting behavior at an unprecedented level, thus enabling the design of specific characteristics in terms of radiated EM field [3].

N. Decarli is with the National Research Council - Institute of Electronics, Computer and Telecommunication Engineering (CNR-IEIIT), and WiLab-CNIT, Bologna (BO), Italy (e-mail: nicolo.decarli@ieiit.cnr.it). D. Dardari is with the Dipartimento di Ingegneria dell’Energia Elettrica e dell’Informazione “Guglielmo Marconi” (DEI), and WiLab-CNIT, University of Bologna, Cesena Campus, Cesena (FC), Italy, (e-mail: davide.dardari@unibo.it).

This work was sponsored, in part, by Theory Lab, Central Research Institute, 2012 Labs, Huawei Technologies Co., Ltd.

The use of millimeter-wave and terahertz technologies jointly with large antennas poses new challenges and opportunities at the same time, since traditional models based on the assumption of far-field EM propagation fail [10], [11]. Recently, [12] discussed how multiple *communication modes* can be obtained especially when operating in the near-field region. These communication modes correspond to parallel and orthogonal channels that can be realized between a couple of antennas, thus capable of significantly enhancing the channel capacity. Despite the concept of communication modes is well known especially in optics and in guided EM propagation [13], its exploitation for radio communication received only a little attention so far. This is mainly because, for the time being, radio communication systems have been realized with relatively small antennas and using low frequencies; in such a case, only one communication mode is generally available, corresponding to a plane wave traveling from the transmitting to the receiving antenna. Therefore, the line-of-sight (LOS) link capacity is limited, and multi-path propagation is usually exploited by multiple-input multiple-output (MIMO) antenna arrays to enhance the number of parallel channels (modes), namely the degrees of freedom (DoF) of communication. Unfortunately, due to the trend of adopting even increasing frequencies, multi-path tends to become sparse and LOS propagation (e.g., using pencil-like beams) becomes predominant, thus limiting the possibility of exploiting multi-path propagation to activate multiple communication modes. For this reason, there is a great interest in exploiting new methods for enhancing the communication DoF, even in LOS, especially considering the characteristics of propagation in the near field arising from the use of large antennas and high frequency bands.

A. State of the Art

When the paraxial approximation holds (i.e., antennas are parallel, oriented towards their maximum of the radiation intensity, i.e., boresight direction, and small with respect to the link distance), analytical results for the number of communication modes are known, and the corresponding exciting functions at transmitting and receiving antenna side can be written in closed form [14]. In particular, the number of communication modes and the relative coupling intensity are related to the geometry of the scenario (dimensions and shape of the antennas, link distance) and to the operating frequency [14]. Unfortunately, as discussed in [12], the known results for the number of communication modes (i.e., the DoF) cannot be adopted when the link distance becomes comparable to the antenna size, condition that can happen with the use of LIS and IRSs. In such a case, ad-hoc models must be considered also for describing the path loss between antennas, since traditional methods (e.g., the well-known Friis formula) do not capture properly the propagation phenomenon in the near-field region [11], [12]. Moreover, if the assumptions of the paraxial approximation are not fulfilled, no closed-form solutions for the definition of communication modes are known, at the best of authors' knowledge. In the general case, the derivation of the communication modes can be realized by resorting to numerical simulations, which can be not practical for antennas of large size, especially for run-time operations, and do not allow to get insights about the effects of the different system parameters. Thus, new and easy methods for the definition of these communication modes must be investigated.

In the last years, practical methods for activating multiple communication channels also in LOS have been proposed. For example, [15] introduces the continuous aperture phased (CAP)-MIMO technique capable of generating several orthogonal beams in the angular domain using aperture antennas with high flexibility in shaping the EM

wavefront. If the operating frequency is high, for example in the millimeter-wave band or even in the terahertz band, very narrow beams can be realized [16], thus a single aperture antenna much larger than the operating wavelength can capture some of the beams, then allowing multi-mode communication. Unfortunately, the number of communication modes is limited when antennas are small compared to the link distance (e.g., in the far field). Other studies showed the potential of realizing multiple channels when antenna arrays are located at closer distance each other (short-range MIMO), even in LOS thus without the need of exploiting multi-path propagation [17]–[19]. However, a classical point-wise definition of antenna arrays consisting of a finite number of antenna elements, equi-spaced at $\lambda/2$ to make mutual coupling negligible, has been considered. This translates into a sampling of the continuous-space EM channel and continuous signals (propagating waves) according to a specific placement of the array's elements [20], which cannot capture the ultimate limits offered by the wireless channel and exploitable by metamaterials, as recently envisioned under the holographic communication concept [10].

Other practical methods proposed in the last years are based on the generation of orbital angular momentum (OAM) beams, but they assume frequently large distance among the antennas and paraxial conditions [21]–[24]. Moreover, it has been shown that the maximum number of communication modes is limited also using these techniques [13]. Despite the method for realizing multiple communication modes, the traditional results valid under paraxial approximation cannot be adopted for more general configurations or in the near field, and the number of communication modes related to traditional expressions is, in general, overestimated [12].

B. Contributions

In this paper, starting from the analytical formulation leading to the optimum strategy for establishing the communication modes between a couple of antennas, we define a practical method for approximating them. The proposed method exploits the multi-focusing capability of large antennas [25]–[27] in the near-field region. In particular, focusing will be proposed to create orthogonal beams on the receiving antenna. It will be shown that, using focusing in the near field, the number of communication modes is approximatively equal to that using optimal beams obtained from EM simulations. Moreover, it is shown that the number of communication modes corresponds to the maximum number of diffraction-limited focused-beams that can be realized on a screen (i.e., a receiving antenna) by using a certain aperture (i.e., a transmitting antenna) as commonly assumed in optics under paraxial approximation and at large distance [13]. Closed-form solutions will be provided for the case of communication between a LIS and a smaller antenna, that is, a small intelligent surface (SIS), which is of great interest as practical case of communication between a fixed large antenna and a mobile user with a handheld terminal.

The main contributions of the paper can be summarized as follows:

- Proposal of a method based on diffraction theory and use of focusing capability of large antennas for generating multiple orthogonal beams, corresponding to practical communication modes, even in the near-field region;
- Derivation of closed-form approximate solutions for the definition of communication modes (basis set) in the case of communication between a LIS and a SIS, considering both the uplink and downlink scenarios;
- Presentation of novel closed-form expressions for the number of communication modes capable of providing the correct number for any configuration (not only under paraxial approximation) and even in the near-field

region;

- Review of traditional results valid under paraxial approximation in the near-field and far-field regions, showing that they can be obtained as particular cases of the proposed method;
- Discussion of the operating zones around a transmitting antenna, depending on the geometry and operating frequency conditions, in order to explain easily where a capacity gain using multiple communication modes can be obtained.

The remainder of the paper is organized as follows. Sec. II describes the scenario we consider and briefly reviews the theoretical foundations behind the communication through multiple communication modes. Then, Sec. III introduces the approximate method we propose, capable of defining multiple practical communication modes even in the near-field region; in the same section, particular cases of interest are discussed and easy closed-form expressions for the available number of communication modes are provided under different conditions. Sec. IV revises the regions of space around antennas in light of the theory developed, thus discussing the conditions for activating multiple communication modes. Numerical results are presented in Sec. V, and Sec. VI concludes the paper.

II. SCENARIO AND PROBLEM FORMULATION

A. Scenario Considered

We consider two linear aperture antennas (i.e., segments in space), according to Fig. 1. The receiving antenna has a length L_R and is oriented along the y axis, with center in $y = y_c$. The transmitting antenna has a length L_T and is rotated of an angle θ with respect to the y axis, considering a positive angle for counterclockwise rotation. The origin of the reference system is in the center of the transmitting antenna, with the z axis oriented in the horizontal direction and the y axis oriented in the vertical direction. The distance between the centers of the two antennas is d_c , and the horizontal projection of such a distance on the z axis is z . For further convenience, we consider η the coordinate along the transmitting antenna, with upward positive direction along its orientation when $\theta = 0$, and y the vertical coordinate along the receiving antenna. The two antennas are assumed lying on the same plane (2D analysis), and any relative orientation and displacement among the two antennas are considered with y_c and θ . This assumption can serve as benchmark for more complicated scenarios and to understand the key concepts behind the generation of multiple communication modes that will be discussed. Notice that, recently, practical schemes exploiting linear antennas, namely *radio stripes*, have been proposed and have several interesting practical implications [28].

We denote with \mathbf{s} in \mathcal{S}_T and \mathbf{r} in \mathcal{S}_R a couple of vectors pointing from the origin O towards a point on the transmitting and receiving antennas, being \mathcal{S}_T and \mathcal{S}_R , the set of points belonging to the transmitting and receiving antennas, respectively. The distance between the two points on the transmitting and receiving antennas is indicated with r , so that

$$r = |\mathbf{r} - \mathbf{s}| = \sqrt{(z + \eta \sin \theta)^2 + (y - \eta \cos \theta)^2} \quad (1)$$

where $|\cdot|$ is the Euclidean norm. The explicit dependence of r on z, y, η, θ is omitted to simplify the notation.

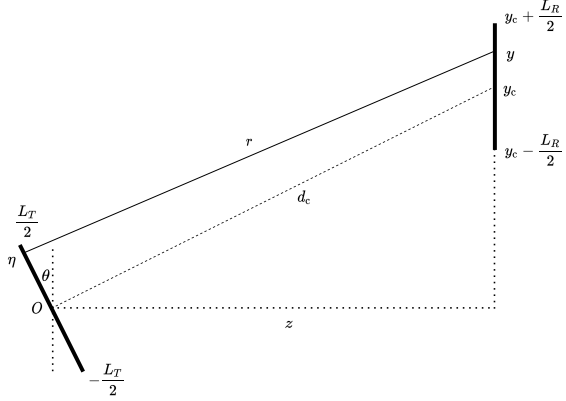


Fig. 1. The considered scenario.

In the following, we consider the antennas as ideal apertures in free space, where there is the complete freedom of drawing any current distribution on their surface (holographic capability). In fact, an analysis based on dense discrete antenna elements would require a careful characterization of the mutual coupling among the elements which is, in most of cases, feasible only through EM simulations, and it would be stucked to a specific technology. Instead, considering the antenna as a continuum composed of an infinite number of infinitesimal antennas, each producing an outgoing spherical wave with a given amplitude and phase, allows investigating the ultimate limits of the wireless communication without accounting for a specific technology or implementation-related aspects. Notice that such an assumption corresponds to supposing the antenna as an ideal EM source obeying the Huygens-Fresnel principle, where each infinitesimal antenna is a Huygens' source. Although the EM field is a vector quantity, here it is treated, as first approximation, as a complex-valued scalar quantity to simplify the discussion. This is a common approach, frequently adopted in optics, which can be consider valid until all the elements of the discussion (dimension of antennas, distance...) are relatively large with respect to the wavelength [29]. Of course, by considering the field as a vector, additional communication modes could be obtained by exploiting, for example, polarization diversity [13], [20], [30].

B. Communication Modes

Consider a monochromatic source at frequency f_0 , that is, a function $\phi(\mathbf{s})$. This function can describe the current density distribution (amplitude and phase) on the transmitting antenna [12]. At the receiving antenna side, the source function produces a wave (electric field distribution), that is a function $\psi(\mathbf{r})$, which can be obtained, in free-space conditions, as a solution of the inhomogeneous Helmholtz equation, and it is given by [14]

$$\psi(\mathbf{r}) = \int_{S_T} G(\mathbf{r}, \mathbf{s}) \phi(\mathbf{s}) d\mathbf{s} \quad (2)$$

where $G(\mathbf{r}_1, \mathbf{r}_2)$ denotes the *Green function* between points represented by vectors \mathbf{r}_1 and \mathbf{r}_2 , which is

$$G(\mathbf{r}_1, \mathbf{r}_2) = \frac{\exp(-j\kappa|\mathbf{r}_1 - \mathbf{r}_2|)}{4\pi|\mathbf{r}_1 - \mathbf{r}_2|} \quad (3)$$

with $\kappa = 2\pi/\lambda$ indicating the wavenumber and $\lambda = c/f_0$ the wavelength, with c standing for the speed of light. According to (2), at receiver side we can see the effect of the transmitting antenna (source) as a sum of infinitesimally small contributions (Huygens' sources) producing outgoing spherical waves centered on \mathbf{s} over \mathcal{S}_T of initial amplitude/phase given by $\phi(\mathbf{s})$.

By expanding $\phi(\mathbf{r})$ and $\psi(\mathbf{r})$ using any orthonormal basis set complete in \mathcal{S}_T and \mathcal{S}_R , respectively, we have

$$\phi(\mathbf{s}) = \sum_n a_n \phi_n(\mathbf{s}) \quad (4)$$

$$\psi(\mathbf{r}) = \sum_m b_m \psi_m(\mathbf{r}) \quad (5)$$

where the orthonormal conditions ensure that

$$\int_{\mathcal{S}_T} \phi_m(\mathbf{s}) \phi_n^*(\mathbf{s}) d\mathbf{s} = \delta_{mn} \quad (6)$$

$$\int_{\mathcal{S}_R} \psi_m(\mathbf{r}) \psi_n^*(\mathbf{r}) d\mathbf{r} = \delta_{mn} \quad (7)$$

with δ_{mn} indicating the Kronecker delta function, and it is possible to write

$$b_m = \sum_n \xi_{mn} a_n \quad (8)$$

or, in matrix notation,¹

$$\mathbf{B} = \boldsymbol{\Gamma} \mathbf{A} \quad (9)$$

where $\boldsymbol{\Gamma} = \{\xi_{mn}\}$ is the communication operator between transmitting and receiving antennas, $\mathbf{B} = \{b_m\}$ and $\mathbf{A} = \{a_n\}$ and

$$\xi_{mn} = \int_{\mathcal{S}_R} \int_{\mathcal{S}_T} \psi_m^*(\mathbf{r}) G(\mathbf{r}, \mathbf{s}) \phi_n(\mathbf{s}) d\mathbf{s} d\mathbf{r} \quad (10)$$

is the *coupling intensity*. Equation (10) is valid for any choice of the orthonormal basis sets. For a given geometry (space locations of transmitting and receiving antennas, of finite size) it is possible to show that the sum of all the coupling coefficients ξ_{mn} is limited (sum rule) [14], that is

$$\gamma_{RT} = \sum_{mn} |\xi_{mn}|^2 = \frac{1}{(4\pi)^2} \int_{\mathcal{S}_R} \int_{\mathcal{S}_T} \frac{1}{|\mathbf{r} - \mathbf{s}|^2} d\mathbf{s} d\mathbf{r}. \quad (11)$$

This sum is intimately related to the path loss of the channel [12]. In general, each basis function at the transmitting antenna is coupled with more basis functions at the receiving antenna. If the orthonormal basis set is chosen so that the operator $\boldsymbol{\Gamma}$ is a diagonal matrix, a one-to-one correspondence among the TX and RX basis functions is established. Formally, we have $\boldsymbol{\Gamma} = \text{diag}\{\xi_n\}$ so that the n th basis function $\phi_n(\mathbf{s})$ produces an effect $\xi_n \psi_n(\mathbf{r})$ on the receiving antenna space, where $|\xi_n|$ is the largest possible coupling coefficient, and ξ_1, ξ_2, \dots are (in modulus) in decreasing order on the main diagonal of $\boldsymbol{\Gamma}$. For a well-coupled communication mode (i.e., large $|\xi_n|$), the wave generated by the transmitting antenna impinges the receiving antenna. Differently, for a loosely-coupled communication mode (i.e., small $|\xi_n|$), the wave generated by the transmitting antenna is mostly spread away from the receiving antenna [13].

¹In the sense of Hilbert spaces, thus also considering vectors and matrices of infinite dimension [13].

These basis sets (communication modes) can be found by solving a coupled eigen-function problem, specifically [13]

$$|\xi_n|^2 \phi_n(\mathbf{s}) = \int_{S_T} K_T(\mathbf{s}, \mathbf{s}') \phi_n(\mathbf{s}') d\mathbf{s}' \quad (12)$$

$$|\xi_n|^2 \psi_n(\mathbf{r}) = \int_{S_R} K_R(\mathbf{r}, \mathbf{r}') \psi_n(\mathbf{r}') d\mathbf{r}' \quad (13)$$

where the kernels $K_T(\mathbf{s}', \mathbf{s})$ and $K_R(\mathbf{r}, \mathbf{r}')$ are given by

$$K_T(\mathbf{s}', \mathbf{s}) = \int_{S_R} G^*(\mathbf{r}, \mathbf{s}) G(\mathbf{r}, \mathbf{s}') d\mathbf{r} \quad (14)$$

$$K_R(\mathbf{r}, \mathbf{r}') = \int_{S_T} G(\mathbf{r}, \mathbf{s}) G^*(\mathbf{r}', \mathbf{s}) d\mathbf{s}. \quad (15)$$

More in particular, by solving (12) and (13), the eigenfunctions (basis set) ensure the most accurate approximation of the Green function (3) for any cardinality of the basis set itself.²

From a practical point of view, for finite-size antennas, it is possible to show that the number of significantly non-zero eigenvalues on the main diagonal of Γ is limited. In other words, fixed a couple of antennas, there is a physical limit on the number of communication modes (namely DoF) with significant coupling, after which the coupling intensity falls off rapidly to zero. Such a behavior is well known for the eigenvalues of problems having as eigenfunctions prolate spheroidal wave functions (PSWFs) [31], as obtained by resolving (12) and (13) in the case of linear antennas of small size with respect to the link distance under paraxial approximation (i.e., parallel antennas, with $y_c = 0$, $\theta = 0$ and $L_T, L_R \ll z$) [14]. Then, it is possible to consider a finite number N of basis both at transmitting and receiving antenna side, and hence (9) assumes the usual meaning of vector-matrix product. Under this assumption, it is well known that [14], [15]

$$N \approx \frac{L_T L_R}{\lambda z}. \quad (16)$$

When operating in the far field (i.e., large λz) and in LOS between the antennas, only a single communication mode can be activated ($N = 1$), corresponding to a plane wave traveling from the transmitting to the receiving antenna.³ Notice that (16) is verified only according to the geometric paraxial approximation assumption, without any requirement for the operating frequency; thus, with the increasing of the operating frequency (i.e., smaller wavelength), multiple communication modes become feasible, even at relatively large distance among the antennas. This opportunity can be exploited with beamspace MIMO, realizing orthogonal beams in the angular domain between the transmitting and receiving antennas [15]. The different beams can be obtained by adopting linear phase profiles on the transmitting antennas (i.e., beam steering), by selecting properly the beam-pointing angular directions in order to ensure orthogonality. In fact, a constant phase profile translates into a beam directed on the antenna

²See [12] for a more detailed discussion.

³Equation (16) should be intended as the closest integer. The limit for large z in (16) is 0, however a single communication mode can be always activated provided that the receiver noise is low if compared to the relative coupling intensity (i.e., with respect to the received power). Moreover, it is known that N in (16) is a conservative estimate, and the number of well-coupled modes is generally between N and $N + 1$ [15].

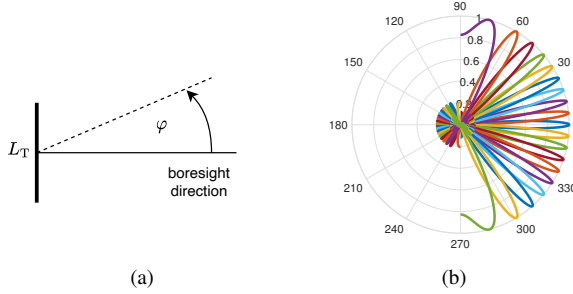


Fig. 2. Far-field orthogonal beams for $f_0 = 28$ GHz and $L_T = 10$ cm.

boresight (i.e., the *optical axis* of the transmitting antenna, making a parallelism with optics). Specifically, a linear phase profile, that is a transmitting function $\phi(\eta)$ in the form

$$\phi(\eta) = \text{rect}\left(\frac{\eta}{L_T}\right) e^{-j\frac{2\pi}{\lambda}\eta \sin \varphi} \quad (17)$$

with $\text{rect}(x) = 1$ for $x \in [-0.5, 0.5]$ and 0 otherwise, realizes, in the far field, a beam in the direction (angle) φ with respect to the antenna boresight; (17) generalizes the well-known results for beam steering with linear arrays [32] in the holographic case considering a continuous antenna. In fact, we can see (17) as the array factor produced by the Huygens' sources on the transmitting antenna; $\varphi = 0$ is obtained with all the sources in-phase (broadside array, corresponding to a main lobe perpendicular to the direction of the array), while $\varphi = \pm\pi/2$ is obtained by imposing a phase difference equal to the separation of adjacent sources scaled by λ (end-fire array, corresponding to a main lobe along the direction of the array). The beamspace technique can be adopted only when the antennas are small compared to the propagation distance; unfortunately, such a condition may correspond to a very limited number of communication modes, due to the small coupling among the antennas [15]. In fact, a transmitting antenna can realize, in the far field, up to $N_{\max} = 2L_T/\lambda$ orthogonal beams in a hemisphere (i.e., for $-\pi/2 \leq \varphi \leq \pi/2$), as depicted in Fig. 2.⁴ However, only a fraction $N \ll N_{\max}$ will intercept the receiving antenna of size L_R thus coupling properly with the transmitting antenna [15].

When the distance between the transmitting antenna and the receiving antenna decreases, propagation takes part in the near-field region. Diffraction theory developed in optics, describes the beams obtained in such propagation condition using the Fresnel integrals [29]. Assuming the beam steering transmitting function in (17) with $\varphi = 0$, the corresponding beam on the receiving antenna region, assumed centered in the boresight direction, is reported in Fig. 3; in particular, the different beams obtained in the figure are shown for different values of the distance among the transmitting and receiving antennas considering $f_0 = 28$ GHz and a transmitting LIS of $L_T = 1$ m. It can be noticed how, in this case, it is easy to have very wide beams even at practical operating distances⁵ (1 \div 10 m in the example of Fig. 3); therefore, a mobile terminal equipped with a relatively small antenna could not intercept much of the beam, thus making hard to activate multiple communication modes (very low coupling due to a wave mainly

⁴In Fig. 2, $N_{\max} = 2L_T/\lambda = 18.7$ and, in fact, 19 beams are shown.

⁵Notice that, at the distance considered, the beam width is close to the transmitting antenna size L_T .

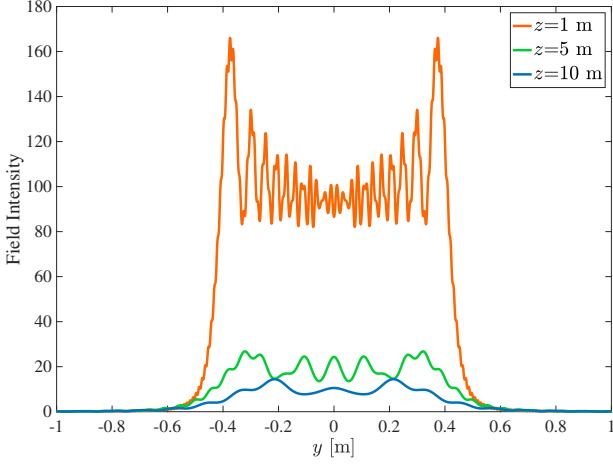


Fig. 3. The Fresnel beams in the near-field region for $y_c = 0\text{ m}$, $\theta = 0^\circ$, $f_0 = 28\text{ GHz}$ and a LIS with $L_T = 1\text{ m}$.

dispersed away from the receiving antenna). In this case, classical beam steering techniques may be extremely inefficient, and one should resort to the exact solution to the coupled eigenfunction problem in (12)-(13).

For a generic setup, even in the near field, finding the solution of the coupled eigenfunction problem in (12)-(13) requires extensive and sometimes prohibitive simulations if large antennas are considered. In particular, a discretization into a fine mesh of the transmitting and receiving antenna regions can be realized, then solving numerically the eigenfunctions problem and applying singular value decomposition (SVD) which might lead to huge matrices. For this reason, there is a great interest in finding simple ways to define the communication modes. A practical method extending the beamspace techniques also in the near field will be presented in Sec. III.

III. PRACTICAL DERIVATION OF THE BASIS SETS

A. General Case

In this section, we propose a method for the definition of a practical basis set, thus approximating optimal solutions without the need of evaluating numerically (12) and (13). Moreover, the proposed solution will be specified in particular cases of interest leading to analytical solutions, thus providing insights into the problem, not otherwise available with numerical solutions.

Let us consider the kernel $K_R(\mathbf{r}, \mathbf{r}')$ in (15), by declining it in the scenario described in Fig. 1. In this case, we can write $G(\mathbf{r}, \mathbf{s})$ as a function of $r = |\mathbf{r} - \mathbf{s}|$ given by (1). In order to simplify the notation, in the following we will denote the Green function (3) with $G(r)$, omitting the explicit dependence of r on y and η .

Defining $r' = \sqrt{(z + \eta \sin \theta)^2 + (y' - \eta \cos \theta)^2}$, we have

$$\begin{aligned} K_R(y, y') &= \int_{-L_T/2}^{L_T/2} G(r) G^*(r') d\eta \\ &= \int_{-L_T/2}^{L_T/2} \frac{e^{-j\kappa\sqrt{(z + \eta \sin \theta)^2 + (y' - \eta \cos \theta)^2}}}{4\pi\sqrt{(z + \eta \sin \theta)^2 + (y' - \eta \cos \theta)^2}} \times \frac{e^{j\kappa\sqrt{(z + \eta \sin \theta)^2 + (y' - \eta \cos \theta)^2}}}{4\pi\sqrt{(z + \eta \sin \theta)^2 + (y' - \eta \cos \theta)^2}} d\eta. \end{aligned} \quad (18)$$

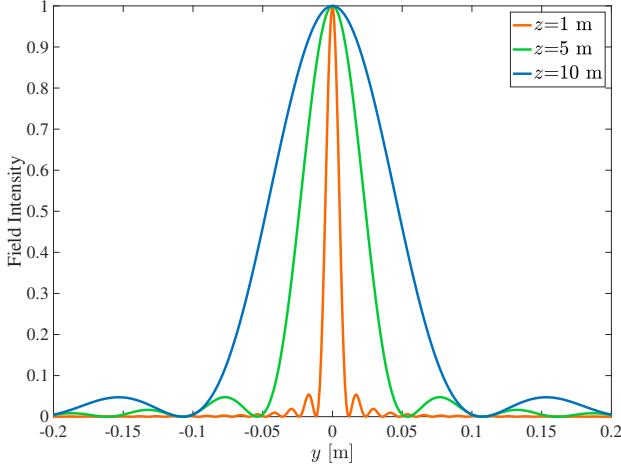


Fig. 4. The (normalized) focused-beams in the near field region realized according to (20) for $y_c = 0$ m, $\theta = 0^\circ$, $f_0 = 28$ GHz and a LIS with $L_T = 1$ m.

For practical operating distances among the antennas, in (18) we can approximate the denominators with simply d_c , while such an approximation cannot be adopted for the numerators due to the interference effects produced by the phase terms. Then,

$$K_R(y, y') \approx \quad (19)$$

$$\frac{1}{(4\pi d_c)^2} \int_{-L_T/2}^{L_T/2} \exp\left(-J\kappa\sqrt{(z + \eta \sin \theta)^2 + (y - \eta \cos \theta)^2}\right) \times \exp\left(J\kappa\sqrt{(z + \eta \sin \theta)^2 + (y' - \eta \cos \theta)^2}\right) d\eta.$$

On the right hand side of the integral in (19), we recognize the phase profile required at the transmitting antenna to focus its energy on the point y' at the receiving antenna (focal point), that is, to have all the wave components (infinitesimal outgoing spherical waves produced by Huygens' sources on the transmitting antenna) summing up in-phase at the point of coordinates (z, y') , thus compensating for the phase delay introduced by the propagation. Using focusing, we have an increase of the EM power density in a size-limited region of the space close to the focal point, if located relatively close to the antenna. In fact, differently from the beam steering, which consists in concentrating the radiated energy towards a specific direction in the far field (corresponding to focusing at infinite distance), operating in the near field allows concentrating the field on a specific point in the space [26], as will be further discussed in the Sec. IV. With reference to Fig. 1, we define the focusing function⁶ at the transmitting antenna required to focus at the point y' on the receiving antenna as

$$F_T(\eta)|_{y'} = \text{rect}\left(\frac{\eta}{L_T}\right) e^{J\frac{2\pi}{\lambda}\sqrt{(z+\eta \sin \theta)^2 + (y'-\eta \cos \theta)^2}} \quad (20)$$

At the receiving antenna side the field is given by (2), that is

$$\psi(y)|_{y'} = \int_{-L_T/2}^{L_T/2} G(r) F_T(\eta)|_{y'} d\eta \quad (21)$$

⁶Here, differently from near-field focused (NFF) antenna arrays [26], we have a continuous phase profile with η (holographic assumption, with the LIS considered as an ideal aperture antenna).

where we used the notation $\psi(y)|_{y'}$ to identify the field distribution in the case we used a phase profile at transmitting antenna side to focus the radiation towards y' on the receiving antenna. Fig. 4 reports the beams obtained on the receiving antenna (i.e., functions $|\psi(y)|$ given by (21)) using focusing according to (20) for $y' = 0$, $\theta = 0$, and the same distance set considered in Fig. 3. It is immediate to notice that the focusing function changes completely the Fresnel beams of Fig. 3, into much more concentrated functions.⁷ Then, even a mobile user equipped with a relatively small antenna could intercept the beam, resulting in a good coupling among transmitting and receiving antennas. This behavior suggests the possibility of implementing a beamspace-like multi-mode communication using focusing functions in the form (20) instead of beam steering functions in the form (17) when operating in the near field.

Now we notice that (21) is formally identical to the kernel (19), except for a multiplicative factor. Moreover, it is possible to write the kernel as the product of a focusing function towards y' and the complex conjugate of a focusing function towards a generic y , that is

$$K_R(y, y') = \frac{1}{(4\pi d_c)^2} \int_{-L_T/2}^{L_T/2} (F_T(\eta)|_y)^* F_T(\eta)|_{y'} d\eta. \quad (22)$$

If (22) is zero for any couple of focusing functions towards y' and y , for some $y' \neq y$, we obtain the same condition (6) that we have to meet for orthogonal basis sets. More specifically, by assuming that the first base function at transmitting side is defined as the focusing function towards y' , we ask how far we have to move along the direction y (i.e., on the receiving antenna) to have orthogonality with respect to such a focusing function. Once y is found, the second base function at the transmitting side will be a focusing function towards that specific y . The process can be iterated until it is not possible to find a new y inside the receiving antenna capable of fulfilling the orthogonality condition. The orthonormal version can be obtained by dividing each base function by a scale factor $\sqrt{L_T}$. Thus, focusing functions in the form (20), with proper choices of the points y' , can form basis sets at the transmitting antenna side.

From a practical point of view, we have to construct the functions starting from a particular point at the receiving antenna. A viable way consists in assuming a first base function at the transmitting antenna side as the focusing function towards the center y_c of the receiving antenna, thus using (z, y_c) as focal point, that is

$$\phi_0(\eta) = \frac{1}{\sqrt{L_T}} F_T(\eta)|_{y_c}. \quad (23)$$

The next step is to move along y in positive direction until a null (or a local minimum from a practical point of view) of the kernel $K_R(y, y_c)$ in (19) (i.e., an orthogonal focusing function) is found, corresponding to point y_1 ; a new base is then constructed as a focusing function towards that point. The process is iterated with all the other nulls of $K_R(y, y_c)$ until the focal point falls outside the receiving antenna. Then, the same process is repeated for the negative direction starting from the receiving antenna centre.

The method defines basis functions at the transmitting antenna. The effect at the receiving antenna is given, for every focusing function, by (21). An example of the beams realized at the receiving antenna with the proposed approach is reported in Fig. 5. In particular, a receiving antenna of size $L_R = 20$ cm is assumed, with the other

⁷Notice the different scale on the horizontal axis for Fig. 4 with respect to that of Fig. 3.

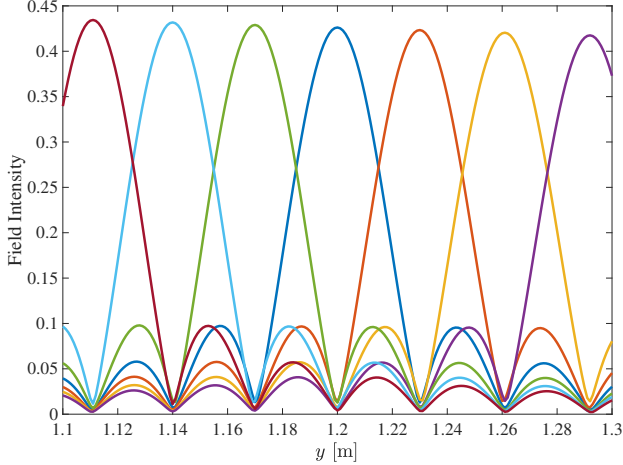


Fig. 5. The $N = 7$ beams obtained using focusing according to (20) in the near-field region for $y_c = 1.2$ m, $\theta = 20^\circ$, $z = 2$ m, $f_0 = 28$ GHz and a LIS with $L_T = 1$ m. A receiving antenna of size $L_R = 20$ cm is assumed.

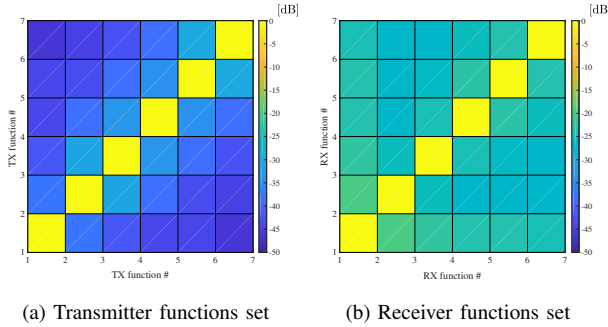


Fig. 6. Numerical check of orthogonality at transmitter and receiver side (worst-case -23 dB at the transmitting antenna side, and -16 dB at the receiving antenna side).

geometrical parameters reported in the caption (non-paraxial case). It can be noticed that $N = 7$ beams according to (21) can be realized. It is worth to underline that finding orthogonal functions does not ensure that these can be used to form (orthogonal) communication modes, that is, solutions of the eigenfunction problem (12)-(13). Orthogonality among the functions at transmitting and receiving antenna side was checked numerically and it is reported in Fig. 6. It can be noticed a good orthogonality even at the receiving antenna side (around -20 dB) for the considered example. Thus, $N = 7$ practically-orthogonal communication modes can be realized, thus boosting significantly the system capacity between the transmitting antenna equipped with the LIS and the user equipped with a smaller antenna here considered. Moreover, the close orthogonality ensures that the basis functions constructed starting from focusing functions, even though not optimal in general, provide almost the same number of communication modes when using the optimal basis set solution of (12)-(13), as it will be discussed more in detail later.

Notice that, with the choice made on the specific focusing functions, each beam (i.e., each basis function at receiving antenna side) is centered in the first null corresponding to the adjacent beam (the adjacent basis function

at the receiving antenna side, see Fig. 5); this corresponds to the Rayleigh criterion for resolution of optical images [29], also known as Rayleigh spacing (usually denoted in the angular domain, that is in the far field in [33]). Thus, the number of communication modes equals the maximum number of diffraction-limited focused-beams, that can be obtained at the receiving antenna side, produced by an aperture of size equal to the size of the transmitting antenna, without mutual interference. As happens in diffraction theory and experiments, larger apertures (i.e., larger antennas) produce narrower beams (i.e., more concentrated basis functions) at the receiving antenna side; thus, the wider the transmitting and receiving antennas are, the higher is the number of communication modes that can be established, as expected.

Focusing functions in the near field allow realizing a beamspace-MIMO-like approach similarly to what done in the angular domain (far field) with beam steering. Here, orthogonality cannot be considered in the angular domain, since in the near field the transmitting antenna beam pattern changes with the distance due to the spherical wavefront propagation. Differently, orthogonality is ensured on the receiving antenna region. It has to be remarked that, from an implementation point of view, the realization of beams with focusing requires the knowledge of relative position and orientation among the antennas; this can be realized with high accuracy by exploiting the information carried by the spherical wavefront [34], [35].

Summarizing:

- The approach described allows defining orthogonal functions on the transmitting antenna using focusing functions (phase profiles) towards the nulls of the kernel $K_R(y, y_c)$;
- It can be verified numerically that the focusing functions produce practically-orthogonal beams on the receiving antennas in several cases of interest, as will be discussed in depth in Sec. V. Thus, we are defining multiple communication modes.

The functions proposed are not the optimum, which is obtained by solving (12)-(13) leading to perfectly orthogonal functions, thus diagonalizing Γ . However, the good level of orthogonality verified numerically allows defining practical communication modes, and it will be shown that their numbers equal that of optimum solutions.

In the following sections:

- The proposed approach will be declined to particular but practical configurations leading to analytical solutions both at transmitting and receiving antenna side;
- Traditional results obtained as approximate solutions in the paraxial case will be revised in light of the proposed method.

In particular, we now derive easy closed-form expressions for the basis functions at transmitting and receiving antenna side and for the number of communication modes considering the communication between an antenna of small size, and a large intelligent antenna.

B. Communication Modes between a SIS and LIS: Uplink

As first, we consider a small transmitting antenna (i.e., uplink scenario). In this case, we can adopt the Maclaurin series expansion at the first term for the distance r as a function of the variable η , in the numerators (phase terms)

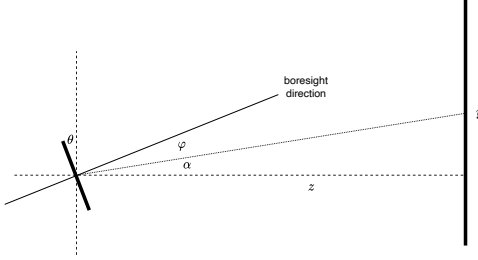


Fig. 7. Geometry of communication between a SIS and a LIS (uplink).

of (18)-(22), around the antenna center $\eta = 0$, that is

$$\frac{2\pi}{\lambda} r(\eta) \approx \frac{2\pi}{\lambda} \left[r(0) + \eta \frac{\partial}{\partial \eta} r(\eta) \Big|_{\eta=0} \right]. \quad (24)$$

Using (24), it is possible to write the focusing function $F_T(\eta)|_y$ in (20) as

$$F_T(\eta)|_y = \text{rect}\left(\frac{\eta}{L_T}\right) e^{j \frac{2\pi}{\lambda} \frac{\sin \theta - \gamma \cos \theta}{\sqrt{1+\gamma^2}} \eta} \quad (25)$$

whose derivation is reported in Appendix A, where $\gamma = y/z$. It is immediate to see that we have obtained a phase profile of the same form of (17), that is, linear with η . Thus, this corresponds to a beam steering phase profile allowing to concentrate the radiated energy towards a specific direction in the far field, that is, angle φ , with respect to the (small) transmitting antenna. In particular, the angle φ obeys to

$$\rho = -\sin \varphi = \frac{\sin \theta - \gamma \cos \theta}{\sqrt{1+\gamma^2}} \quad (26)$$

where the explicit dependence of ρ from y, z and θ is omitted to simplify the notation. By writing $\gamma = y/z = \tan \alpha$, with simple trigonometric manipulations, it is easy to show that φ in (26) corresponds to an angle $\varphi = \alpha - \theta$, which is expected, since the focusing function was constructed to focus the radiated energy towards a point (z, y) on the receiving antenna, also considering a generic transmitting antenna orientation θ (see Fig. 7). Thus, beam steering in the direction of the focal point is realized. In this case, the focusing behavior degenerates into a beam steering operation, since the small dimension of the transmitting antenna does not provide the focusing capability (or equivalently, the near-field region of such a transmitting antenna, where focusing is feasible, is small, as it will be discussed more in detail in Sec. IV).

We can now exploit approximation (24) to rewrite the kernel (22) or equivalently the received function (21), which are the same except for a multiplicative factor, considering the focusing towards (z, y_c) , obtaining

$$K_R(y, y_c) \approx \frac{1}{(4\pi d_c)^2} \int_{-\infty}^{\infty} \text{rect}\left(\frac{\eta}{L_T}\right) e^{-j \frac{2\pi}{\lambda} (\rho - \rho_c) \eta} d\eta \quad (27)$$

where ρ_c is obtained from (26) by considering the steering direction towards y_c in the receiving antenna. Then, (27) corresponds to the Fourier transform of $\text{rect}(\eta/L_T)$ evaluated at $(\rho - \rho_c)/\lambda$, so that

$$K_R(y, y_c) \approx \frac{L_T}{(4\pi d_c)^2} \text{sinc}\left(\frac{L_T}{\lambda} (\rho - \rho_c)\right) \quad (28)$$

where $\text{sinc}(x) = \sin(\pi x)/(\pi x)$. The kernel, or equivalently the beam at the receiving antenna side, is a space-varying sinc function of y . Under the hypothesis of steering towards y_c , it is then possible to find orthogonal steering functions for values of y corresponding to integer values of $\frac{L_T}{\lambda}(\rho - \rho_c)$, that is

$$y_n = z \tan \left[\arcsin \left(-\frac{\lambda}{L_T} n - \rho_c \right) + \theta \right], \quad |n| = 1, 2, \dots . \quad (29)$$

Thus, by assuming a first beam directed towards (z, y_c) , from (29) the allowed set of integers n must satisfy

$$-1 \leq \frac{\sin \theta - \frac{y_c}{z} \cos \theta}{\sqrt{1 + \left(\frac{y_c}{z} \right)^2}} + \frac{\lambda}{L_T} n \leq 1 \quad (30)$$

that for the particular case of a parallel receiving LIS in the boresight direction ($\theta = 0$ and $y_c = 0$) simplifies to

$$-\frac{L_T}{\lambda} \leq n \leq \frac{L_T}{\lambda} \quad (31)$$

corresponding to a maximum number of $2L_T/\lambda$ beams in the hemisphere, which is the same result discussed Sec. II-B. Among the indexes n of (30), it is necessary to evaluate which of them correspond to beams intercepting the receiving LIS, thus leading to good coupling among the antennas. Formally, by defining \mathcal{I} the set of indexes corresponding to well-coupled modes, we have

$$\mathcal{I} = \{n\} : y_c - \frac{L_R}{2} < y_n < y_c + \frac{L_R}{2} \quad (32)$$

and $N = |\mathcal{I}|$, where $|\cdot|$ stands for the cardinality of a set.

Equation (29) does not give immediate insights in its general form. However, considering parallel antennas ($\theta = 0$) and exploiting $\tan \arcsin x = x/\sqrt{1+x^2}$, we can write

$$y_n = z \frac{1}{\sqrt{1 - \left(\frac{\frac{y_c}{z}}{\sqrt{1 + \left(\frac{y_c}{z} \right)^2}} - \frac{\lambda}{L_T} n \right)^2}} \left(\frac{\frac{y_c}{z}}{\sqrt{1 + \left(\frac{y_c}{z} \right)^2}} - \frac{\lambda}{L_T} n \right) \quad (33)$$

for $n \in \mathcal{I}$, where it is evident the stretching of the sinc lobes while moving along y . From (33) we can observe several facts:

- The distance among the nulls increases with z . This is expected, since larger distance produces wider beams, thus the density of beams decreases.
- The distance among the nulls increases with λ . Again, using smaller wavelength is beneficial to concentrate the radiation towards a smaller area on the receiving antenna, thus increasing the number of beams.
- The distance among the nulls decreases with L_T . Also, this fact is expected, since larger antennas can concentrate more efficiently the radiation towards a smaller area on the receiving antenna, thus increasing the number of beams.

Coming back to the general case, we have at the transmitting antenna side

$$\phi_n(\eta) = F_T(\eta)|_{y_n} = \frac{1}{\sqrt{L_T}} \text{rect} \left(\frac{\eta}{L_T} \right) e^{j \frac{2\pi}{\lambda} \frac{\sin \theta - y_n \cos \theta}{\sqrt{1 + y_n^2}} \eta} \quad (34)$$

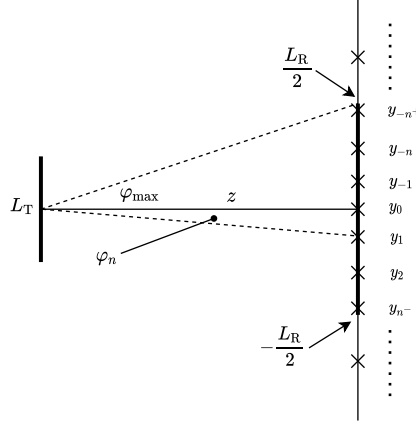


Fig. 8. Relationship among geometry and nulls in the paraxial case.

for $n \in \mathcal{I}$ and with $\gamma_n = y_n/z$ and, at the receiving antenna side

$$\psi_n(y) = K \operatorname{sinc} \left(\frac{L_T}{\lambda} \left(\frac{\sin \theta - \frac{y}{z} \cos \theta}{\sqrt{1 + \left(\frac{y}{z} \right)^2}} - \frac{\sin \theta - \frac{y_n}{z} \cos \theta}{\sqrt{1 + \left(\frac{y_n}{z} \right)^2}} \right) \right) \quad (35)$$

where K is a normalization constant needed to obtain an orthonormal basis.⁸

This result extends the beamspace-MIMO approach for an uplink case between a transmitting SIS and a receiving LIS, behind the traditional paraxial approximation and considering generic orientations among the antennas. At the transmitting antenna side, due to the small size of the antenna, the SIS operates beam steering according to (34) towards specific angles $\varphi_n = \alpha_n - \theta$ with respect to the transmitting antenna boresight, with $\alpha_n = \arctan \gamma_n$. At the receiving antenna side, the LIS correlates the impinging EM field with the n th basis function, that is, space-varying sinc functions according to (35), in order to retrieve the information associated to the n th communication mode.

1) Number of Communication Modes: As specified in (32), the number of communication modes for a generic configuration corresponds to the cardinality of the set \mathcal{I} , that is, the number of nulls of the kernel following inside the receiving antenna of size L_R . We now derive simple closed-form expressions for cases of particular interest.

In case of parallel antennas ($\theta = 0$, $y_c = 0$) we have $\rho_c = 0$ and (29) gives

$$y_n = z \tan \left[\arcsin \left(-\frac{\lambda}{L_T} n \right) \right], \quad |n| = 1, 2, \dots . \quad (36)$$

The number of nulls n^+ in the positive half plane of the receiving antenna ($0 < y_n < L_R/2$), according to Fig. 8, corresponding to indices $n < 0$, is

$$n^+ = n : y_n < \frac{L_R}{2}, \quad n = -1, -2, \dots . \quad (37)$$

⁸Its value is of interest only for the calculation of the coupling intensity of each communication mode.

Due to the symmetry of the configuration, the number of nulls n^- in the negative half plane of the receiving antenna ($-L_R/2 < y_n < 0$) is the same. Then, considering also the beam directed towards $y = 0$, the number of communication modes is

$$N = 1 + n^+ + n^- = 1 + \frac{2L_T L_R}{\lambda \sqrt{4z^2 + L_R^2}} \quad (38)$$

which is obtained by solving (37) with y_n given by (36), as showed in Appendix B. For a very large receiving antenna (limit for $L_R \rightarrow \infty$) we have⁹ $N = 2L_T/\lambda$, which depends only on the size of the transmitting antenna (i.e., the smallest of the two), which is consistent with the results already found in [12]. In fact, an infinite-size receiving antenna, parallel to the transmitting one, would be able to intercept all the beams generated by the SIS (showed for example in Fig. 2), leading to the maximum number of communication modes. Differently, when z is very large, the number of communication modes tends to 1 considering the central beam for $n = 0$, which is the only possible for very large distance, as commonly assumed by traditional radio links in the far field. Finally, for $z \rightarrow 0$, again the limit $N = 2L_T/\lambda$ arises, regardless the size of the receiving antenna. Equation (38) generalizes the well-known result (16) to the case of large antennas, thus also in the case one of the two antennas is in the near field of the other, as discussed in detail in Sec. IV, showing that the number of communication modes cannot increase to arbitrary large values, as erroneously indicated by (16) when applied to any configuration, but intrinsic limits arise.

In case of perpendicular antennas ($\theta = \pi/2$, $y_c = 0$) we have $\rho_c = 1$ and (29) gives

$$y_n = z \tan \left[\arcsin \left(-\frac{\lambda}{L_T} n - 1 \right) + \frac{\pi}{2} \right] = z \cot \left[\arcsin \left(\frac{\lambda}{L_T} n + 1 \right) \right], \quad |n| = 1, 2, \dots . \quad (39)$$

The number of nulls n^+ in the positive half plane of the receiving antenna ($0 < y_n < L_R/2$), corresponding to indices $n < 0$, is given again by (37); however, in this case, $n^- = 0$, since every beam in the upper hemisphere is always coupled with a beam in the lower hemisphere.¹⁰ Thus, considering also the beam directed towards $y = 0$, we have

$$N = 1 + n^+ = 1 + \frac{L_T \left[\sqrt{4z^2 + L_R^2} - 2z \right]}{\lambda \sqrt{4z^2 + L_R^2}} \quad (40)$$

which is obtained by solving (37) with y_n given by (39), as showed in Appendix C. For a very large receiving antenna (limit for $L_R \rightarrow \infty$) we have $N = L_T/\lambda$, which depends only on the size of the transmitting antenna (i.e., the smallest of the two), which is reasonable since only a half of the orthogonal beams (showed for example in Fig. 2) can be intercepted by an infinite-size receiving antenna, perpendicular to the transmitting one. Again, the same limit arises for $z \rightarrow 0$, regardless the size of the receiving antenna.

⁹It should be $N = 2L_T/\lambda + 1$ however, considering a high frequency so that $L_T \gg \lambda$, here and in the following we neglect the factor “+1” for what the limits are concerned. This can be considered, again, a border effect, as also discussed in footnote 4.

¹⁰The antenna was considered as an ideal aperture capable of generating waves in every direction, thus avoiding the need of considering boundary conditions deriving from ground planes. For the symmetry of the Green function, a given phase profile produces a symmetric effect on the two hemispheres around the aperture.

Expressions for a generic θ can be found in closed form and are derived in Appendix D. In particular, we have

$$N = 1 + \begin{cases} \frac{2L_T}{\lambda} \sin(\varphi_{\max}) \cos \theta & \theta \leq \frac{\pi}{2} - \frac{1}{2}\varphi_{\max} \\ \frac{L_T}{\lambda} [\sin(\varphi_{\max} - \theta) + \sin \theta] & \theta \geq \frac{\pi}{2} - \frac{1}{2}\varphi_{\max} \end{cases} \quad (41)$$

where $\varphi_{\max} = \arctan L_R/2z$ (see Fig. 8) for $0 \leq \theta \leq \pi/2$. When $\theta = 0$ and $\theta = \pi/2$, expressions (38) and (40) are obtained. For $L_R \rightarrow \infty$ or $z \rightarrow 0$, the limit for a generic θ is given by

$$N = 1 + \begin{cases} \frac{2L_T}{\lambda} \cos \theta & \theta \leq \frac{\pi}{4} \\ \frac{L_T}{\lambda} (\cos \theta + \sin \theta) & \theta \geq \frac{\pi}{4} \end{cases} \quad (42)$$

2) *Paraxial Case*: We discuss now more in detail the paraxial case. When $\theta = 0$ and $y_c = 0$, the basis set at transmitting antenna side results in

$$\phi_n(\eta) = F_T(\eta)|_{y_n} = \frac{1}{\sqrt{L_T}} \text{rect}\left(\frac{\eta}{L_T}\right) e^{-j\frac{2\pi}{\lambda} \frac{y_n}{\sqrt{1+(\frac{y_n}{z})^2}} \eta} \quad (43)$$

with y_n given by (36) or, in other form,

$$y_n = -z \frac{\lambda}{L_T} \frac{1}{\sqrt{1 - \frac{\lambda^2}{L_T^2} n^2}} n \quad (44)$$

and, at the receiving antenna side

$$\begin{aligned} \psi_n(y) &= K \text{sinc}\left(\frac{L_T}{\lambda} \left(\frac{y_n}{\sqrt{z^2 + y_n^2}} - \frac{y}{\sqrt{z^2 + y^2}} \right)\right) \\ &= K \text{sinc}\left(-\frac{L_T}{\lambda} \frac{y}{\sqrt{z^2 + y^2}} - n\right). \end{aligned} \quad (45)$$

It is also possible to analyze the paraxial case in the angular domain. In fact, by writing $\varphi_n = \arctan(y_n/z)$ (see Fig. 8) we have

$$\varphi_n = \arcsin -\frac{\lambda}{L_T} n. \quad (46)$$

Thus, in a half hemisphere, we have

$$n^{\max} = n : \varphi_n < \frac{\pi}{2} = \frac{L_T}{\lambda} \quad (47)$$

leading to the same result on the maximum number of beams introduced in Sec. II-B. At transmitting antenna side, we have

$$\begin{aligned} \phi_n(\eta) &= F_T(\eta)|_{y_n} = \frac{1}{\sqrt{L_T}} \text{rect}\left(\frac{\eta}{L_T}\right) e^{-j\frac{2\pi}{\lambda} \frac{\tan \varphi_n}{\sqrt{1+\tan^2 \varphi_n}} \eta} \\ &= \frac{1}{\sqrt{L_T}} \text{rect}\left(\frac{\eta}{L_T}\right) e^{-j\frac{2\pi}{\lambda} \sin \varphi_n \eta} \\ &= \frac{1}{\sqrt{L_T}} \text{rect}\left(\frac{\eta}{L_T}\right) e^{j\frac{2\pi}{L_T} n \eta} \end{aligned} \quad (48)$$

which highlights the beam steering phase profile towards angles φ_n ; the orthogonality of the basis function is evident as integer multiple of a phasor. The corresponding beams can be written in the angular domain as $\psi_n(\varphi)$, where $\varphi = \arctan(y/z)$, obtaining from (45)

$$\begin{aligned}\psi_n(\varphi) &= \text{sinc}\left(\frac{L_T}{\lambda}\left(\frac{\tan \varphi_n}{\sqrt{1+\tan^2 \varphi_n}} - \frac{\tan \varphi}{\sqrt{1+\tan^2 \varphi}}\right)\right) \\ &= \text{sinc}\left(-\frac{L_T}{\lambda} \sin \varphi - n\right)\end{aligned}\quad (49)$$

which, for $n = 0$, is the far field antenna pattern of an ideal linear aperture [32]. Then, exploiting the angular domain and the paraxial geometry, the maximum number of communication modes can be found by considering the largest angle sustained by the receiving antenna, which is $\varphi_{\max} = \arctan L_R/2z$ (see Fig. 8). Thus, it is

$$n^+ = n : \varphi_n < \varphi_{\max} \quad (50)$$

whose solution leads to the same result of (38).

C. Communication Modes between a LIS and a SIS: Downlink

When communicating between a transmitting LIS and a receiving SIS, that is in the downlink case (dual case with respect to the discussion of Sec. III-B), the number of communication modes is of course the same, due to the reciprocity of the radio link. Moreover, by using the same basis functions $\psi_n(y)$ developed in Sec. III-B but at transmitting side (large antenna), the effect on the receiving small antenna consists in the complex conjugate of the basis functions $\phi_n(\eta)$.

However, the use of the approach based on focusing at the transmitting side, instead of sinc functions, may bring some advantages from the practical point of view and the possibility to exploit the method described in Sec. III-A both in uplink and downlink.¹¹ For this reason, in this section we investigate the downlink case, where focusing is realized with the transmitting LIS towards the receiving SIS. In this case, the receiving SIS will be likely in the near-field region of the transmitting LIS (see discussion in Sec. IV), so focusing will be realized toward the SIS and we cannot adopt the Maclaurin expansion (24) due to the large size of the transmitting antenna. However, for a parallel SIS on the LIS boresight ($\theta = 0$, $y_c = 0$), it is possible to exploit the Fresnel approximation, as frequently done in optics [29]. In particular, when adopting such an approximation, it is possible to expand the numerators (phase terms) $\sqrt{z^2 + (y - \eta)^2}$ in (18)-(22) using the Maclaurin series at the first term with respect to $(y - \eta)/z$, as

$$z \sqrt{1 + \left(\frac{y - \eta}{z}\right)^2} \approx z \left[1 + \frac{1}{2} \left(\frac{y - \eta}{z}\right)^2\right]. \quad (51)$$

Using (51), it is possible to write the focusing function $F_T(\eta)|_y$ as

$$F_T(\eta)|_y = \text{rect}\left(\frac{\eta}{L_T}\right) e^{j \frac{\pi}{\lambda z} \eta^2} e^{-j \frac{2\pi y}{\lambda z} \eta} \quad (52)$$

where, again, all the phase terms independent of η have been discarded, since the addition of a constant phase shift would not change the focusing behavior. In particular, we have that the focusing function is composed of a

¹¹This translates also in the possibility of using phase-tapering only at the transmitting antenna side.

quadratic term and a linear term.¹² When the focusing point is along the boresight direction (i.e., at $y = 0$), the only quadratic phase term is retained, and the focusing function is simply $F_T(\eta) = F_T(\eta)|_{y=0} = \text{rect}\left(\frac{\eta}{L_T}\right) e^{j\frac{\pi}{\lambda z}\eta^2}$, which is consistent with standard definitions (see, for example [14], [20]). Thus, when a receiving SIS is located in the near field of the LIS and with its center along the boresight direction (paraxial case), we have that

$$\phi_0(\eta) = \frac{1}{\sqrt{L_T}} F_T(\eta) = \frac{1}{\sqrt{L_T}} \text{rect}\left(\frac{\eta}{L_T}\right) e^{j\frac{\pi}{\lambda z}\eta^2}. \quad (53)$$

A second orthonormal function can be constructed starting from (22). We obtain

$$\int_{-L_T/2}^{L_T/2} (F_T(\eta)|_y)^* F_T(\eta) d\eta = \int_{-L_T/2}^{L_T/2} e^{j\frac{2\pi y}{\lambda z}\eta} d\eta \propto \sin \frac{\pi y L_T}{\lambda z} \quad (54)$$

which gives nulls (orthogonal condition) for

$$y_n = n \frac{\lambda z}{L_T}, \quad |n| = 1, 2, \dots. \quad (55)$$

Under the Fresnel approximation, we have found that focusing functions in the form (52) establish, with proper choices of y as in (55) and when normalized by $\sqrt{L_T}$, an orthonormal basis set, whose n th element is

$$\phi_n(\eta) = \frac{1}{\sqrt{L_T}} \text{rect}\left(\frac{\eta}{L_T}\right) e^{j\frac{\pi}{\lambda z}\eta^2} e^{-j\frac{2\pi}{L_T}n\eta}, \quad n \in \mathcal{I}. \quad (56)$$

We now compute the field at the receiving antenna given by basis functions in the form (56). By exploiting (2) and approximation (51), we have

$$\begin{aligned} \psi(y)|_{y_n} &= \frac{1}{4\pi z \sqrt{L_T}} e^{-j\frac{\pi}{\lambda}\left(2z + \frac{y^2}{z}\right)} \int_{-\infty}^{\infty} \text{rect}\left(\frac{\eta}{L_T}\right) e^{j2\pi \frac{y}{\lambda z}\eta} e^{-j\frac{2\pi}{L_T}n\eta} d\eta \\ &= \frac{1}{4\pi z \sqrt{L_T}} e^{-j\frac{\pi}{\lambda}\left(2z + \frac{y^2}{z}\right)} \mathcal{F} \left\{ \text{rect}\left(\frac{\eta}{L_T}\right) e^{-j\frac{2\pi}{L_T}n\eta} e^{2j2\pi \frac{y}{\lambda z}\eta} \right\} \Big|_{f_y = \frac{y}{\lambda z}} \\ &= \frac{\sqrt{L_T}}{4\pi z} e^{-j\frac{\pi}{\lambda}\left(2z + \frac{y^2}{z}\right)} \text{sinc}\left(\frac{L_T}{\lambda z}y - n\right) \end{aligned} \quad (57)$$

where $\mathcal{F}(\cdot)$ indicates the Fourier transform and where now we have $d_c = z$ due to the paraxial approximation. Since the exponential term on the left-hand side of (57) can be considered approximatively constant when $y \ll z$ (small receiving antenna), it is possible to notice that (57) defines a set of orthogonal functions at the receiving antenna side. The n th function is centered at the point y_n given by (55) where the corresponding focusing function was pointing, and the same corresponds to the nulls of the adjacent functions. Then, by scaling (57) by a proper factor, we have¹³

$$\psi_n(y) = \sqrt{\frac{L_T}{\lambda z}} \text{sinc}\left(\frac{L_T}{\lambda z}y - n\right), \quad n \in \mathcal{I} \quad (58)$$

and from (57) the coupling intensity is given by

$$|\xi_n| = \frac{\sqrt{\lambda z}}{4\pi z}, \quad \forall n \in \mathcal{I}. \quad (59)$$

Notice that two adjacent basis functions at the receiving antenna side are spaced by $\frac{\lambda z}{L_T}$. Thus, considering a receiving antenna of size L_R , centered at $y_c = 0$, we have a maximum number of communication modes given by

¹²Expression (52) generalizes the result in the Fresnel region for NFF antenna arrays [26] in the case of a LIS-based antenna.

¹³In (58) we neglect border effects due to the finite-size of the receiving antenna in the normalization term for having orthonormal functions.

(16). After such a number N , the focal points would fall outside the receiving antenna area, thus making impossible to define a further communication mode with a significant level of coupling. This is consistent with well-known results of paraxial approximation (see [13]), but it has been found starting with the specific choice of focusing functions as basis set at transmitting antenna side, instead of resorting to the exact solution of the eigenproblem.¹⁴

Interestingly, by writing $\tan \varphi = y/z$, it is possible to write the basis functions at the receiving antenna side (58) in the angular domain, obtaining

$$\begin{aligned}\psi_n(\varphi) &= \sqrt{\frac{L_T}{\lambda z}} \operatorname{sinc}\left(\frac{L_T}{\lambda} \tan \varphi - n\right) \\ &\approx \sqrt{\frac{L_T}{\lambda z}} \operatorname{sinc}\left(\frac{L_T}{\lambda} \sin \varphi - n\right), \quad n \in \mathcal{I}\end{aligned}\quad (60)$$

where the approximation holds for the condition $y \ll z$, that is for small angles.¹⁵ With (60) it is possible to notice that, using focusing, the same angular pattern of a (small) antenna of size L_T is obtained, as in (49), regardless we are observing the angular pattern in the near field. Basically, focusing modifies the Fresnel beams typical of the near field (e.g., that of Fig. 2), thus an angular pattern changing with the distance from the antenna, into an angular pattern corresponding to the same obtained in the far field (e.g., that of Fig. 2). As the beam width in the far field has an inverse relationship with the antenna size L_T , using focusing the width of the focal spot has an inverse relationship with the antenna size L_T (wider antenna, more concentrated focal spot).

IV. ANTENNA OPERATING ZONES

Traditionally, the space around a transmitting antenna is divided into several regions, depending on the characteristics of the field emitted by the antenna itself. The closest area to the antenna corresponds to the reactive near field, where reactive field components from the source antenna are dominant [32]. Then, by increasing the distance from the antenna, we have the radiating near field, and the far field. The focusing capability exploited in Sec. III for the practical definition of the communication modes is known to be a feature which can be exploited when the focal point is located in the near-field region [26]. The traditional definition of boundary between the near field and the far field corresponds to [32]

$$r_{\text{ff}} = \frac{2D^2}{\lambda} \quad (61)$$

where D is the largest dimension of the transmitting antenna (i.e., L_T according to the definition used in this paper), so it is a function of both the antenna size and the operating frequency. Differently from this definition, in the derivation of Sec. III, several approximations regarded the relation among the size of the antenna and the link distance, regardless the operating frequency. Moreover, when a SIS and a LIS are communicating, as assumed in Sec III-B and Sec. III-C, the boundaries between the respective near-field and far-field regions will be severely different for the two antennas. Thus, the aim of this section is that of discussing the relation among the traditional definitions of the regions of space around antennas, and the number of communication modes that can be realized.

¹⁴Thus, the same limitations of the traditional formulation arise, in the case the transmitting antenna becomes very large (number of communication modes overestimated).

¹⁵In fact, it is known in optics that Fresnel approximation is consistent for small angles only [29].

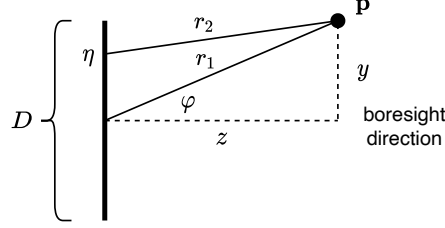


Fig. 9. Geometry for the characterization of the regions of space around an antenna of size D .

A. Near and Far Field

We now briefly review the main differences between propagation in the far field and in the near field. In the far field:

- The angular pattern does not depend on the distance;
- Rays¹⁶ can be considered almost parallel;
- The wavefront can be considered approximatively plane.

In the near field:

- The angular pattern does depend on the distance;
- Rays cannot be considered parallel;
- The wavefront is approximatively spherical.

The definition of the boundary r_{ff} in (61) is obtained by considering a point-like receiver on the boresight direction of the transmitting antenna, and assuming a maximum phase shift corresponding to $\lambda/16$ for outgoing spherical waves arriving at the receiving antenna from the transmitting antenna edges (longest rays) with respect to that from the antenna center (shortest ray) [32]. As alternative, r_{ff} can be considered as the distance for which a radiating point source far apart r_{ff} or more from a receiving antenna of length D would produce a spherical wavefront such that, over the entire D , the phase would vary by no more than $\pi/8$ radians (i.e., $\lambda/16$).

Despite the definition (61) is commonly adopted, a generalization is necessary in the case a receiving antenna is not placed on the boresight direction of the transmitting antenna.

With reference to Fig. 9, consider a transmitting antenna of size D , and a point $\mathbf{p} = (z, y)$, not necessarily located in the antenna boresight direction. We consider two rays, r_1 and r_2 corresponding to the segments from the antenna center and the point \mathbf{p} , and from the generic Huygens' source at the coordinate η of the antenna and the point \mathbf{p} , respectively. We want now to characterize the difference of distance among the two rays, which determines the interference effects in \mathbf{p} of the spherical waves emitted by the two Huygens' sources considered in the transmitting

¹⁶We define a ray as a line that is perpendicular to the wavefront, and that points in the direction of the energy radiated by the antenna (i.e., the receiving antenna).

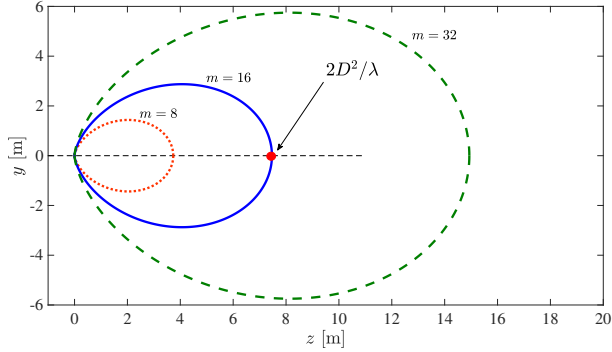


Fig. 10. Boundary between near field and far field for different values of m in (66) (maximum error considered, fraction of λ). Antenna located in $(0, 0)$, oriented along the y axis of size $D = 20$ cm, with $f_0 = 28$ GHz. The red point corresponds to the traditional definition of far-field boundary.

antenna. We have

$$\begin{aligned} r_1^2 &= z^2 + y^2 \\ r_2^2 &= z^2 + (y - \eta)^2. \end{aligned} \quad (62)$$

By exploiting the relations $y = r_1 \sin \varphi$ and $z = r_1 \cos \varphi$, it is possible to write r_2 as a function of r_1 as

$$r_2 = \sqrt{r_1^2 + \eta^2 - 2\eta r_1 \sin \varphi}. \quad (63)$$

Using the Maclaurin expansion at the second order for the path difference, we have

$$\begin{aligned} r_2 &\approx r_1 + \eta \frac{\partial r_2(\eta)}{\partial(\eta)} \Big|_{\eta=0} + \frac{1}{2} \frac{\partial^2 r_2(\eta)}{\partial^2(\eta)} \Big|_{\eta=0} \\ &= r_1 - \eta \sin \varphi + \eta^2 \frac{\cos^2 \varphi}{2r_1}. \end{aligned} \quad (64)$$

If we consider a maximum error for the second order term equal to λ/m , and the worst-condition $\eta = D/2$, we obtain a relation for the distance r_1 from the antenna center to the point \mathbf{p} (i.e., r_{ff}) given by

$$\frac{D^2 \cos^2 \varphi}{8r_1} = \frac{\lambda}{m}. \quad (65)$$

In the boresight direction ($\varphi = 0$), and assuming $m = 16$ as previously discussed, we obtain the traditional relation for the boundary between near field and far field given by (61). Differently, for a generic φ and also considering a generic m , we have

$$r_{\text{ff}} = \frac{mD^2}{8\lambda} \cos^2 \varphi. \quad (66)$$

The 2D shape of the boundary (66) around a transmitting antenna of size $L_T = D = 20$ cm is reported in Fig. 10, considering $m = 16$ (traditional value), $m = 8$ (larger error, thus more conservative definition of near field) and $m = 32$ (smaller error, thus less conservative definition of near field). As a rule of thumb, a transmitting antenna will adopt a beam steering phase profile (i.e., linear phase to concentrate the energy towards a given angle φ) when

transmitting to a receiver located in its far-field region (i.e., above r_{ff} of (66)) and a focusing phase profile (i.e., a phase profile to concentrate the energy towards a specific point in the space (z, y)) when transmitting to a receiver located in its near-field region (i.e., below r_{ff} of (66)). The focusing capability, thus the possibility of establishing multiple communication modes, decreases quickly in the case of:

- Large distance between the transmitter and receiver;
- Large angle with respect to the boresight direction;
- Small antennas;
- Low frequency;

which is consistent with the considerations presented in light of diffraction theory in Sec. III (larger beams, thus smaller number of communication modes).

Of course, these are only conventional boundaries not fixed in space, and the antenna behaviors changes smoothly with the distance. Depending on the relative dimension of these zones for both the transmitting and receiving antennas, a different number of communication modes will be realized.

B. Relationship with the Number of Communication Modes

We now want to discuss the relationship among the antenna regions of Sec. IV-A and the number of communication modes. Let us consider the paraxial case, from which some insights can be drawn in an easier way. In this case, we have small values of φ , so that the traditional expression (61) can be assumed valid. By expressing the size of the transmitting and receiving antenna as a function of their respective boundaries among near field and far field, that is

$$L_T = \sqrt{\frac{\lambda r_{\text{ff}}^{(T)}}{2}}, \quad L_R = \sqrt{\frac{\lambda r_{\text{ff}}^{(R)}}{2}} \quad (67)$$

it is possible to write relation (16) as

$$N = \frac{\sqrt{r_{\text{ff}}^{(T)}} \sqrt{r_{\text{ff}}^{(R)}}}{2z}. \quad (68)$$

If two antennas of the same size are used (e.g., for a point-to-point radio link), so that $r_{\text{ff}}^{(T)} = r_{\text{ff}}^{(R)} = r_{\text{ff}}$, it is immediate to observe that a single communication mode ($N = 1$) is obtained at least up to $z = r_{\text{ff}}/2$. Thus, for antennas of the same size, placing the antenna within their boundary between near field and far field is a necessary condition to establish multiple communication modes. In general, $N > 1$ can be realized when $z < L_T L_R / \lambda$ or, equivalently, multiple communication modes can be established only if antennas are placed at a distance much smaller than their boundary between near field and far field. As presented in Sec. III-B, a transmitting SIS can also establish multiple communication modes with a receiving LIS, by considering a beam steering phase profile (i.e., linear phase); in fact, despite the receiving LIS is likely in the far field of the transmitting SIS, the transmitting SIS is likely in the near field of the LIS. Then, to correctly determine the number of communication modes that can be established by a couple of antennas of any dimension, it is fundamental to consider the operating zones of both transmitting and receiving antennas. The boundaries of the near-field and far-field regions for the configuration

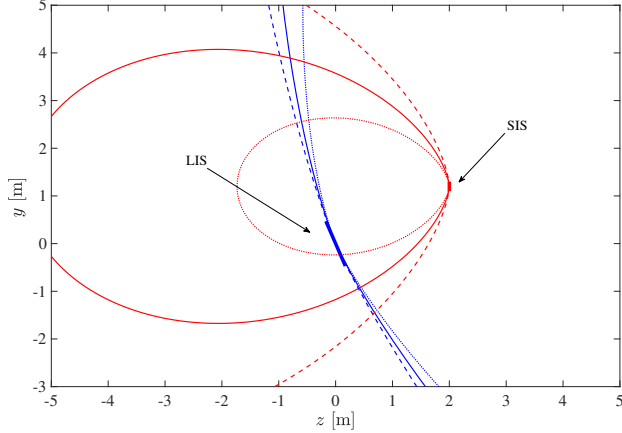


Fig. 11. Boundary between near field and far field for different values of $m = 8, 16, 32$ in (66) for both a transmitting LIS (in red) of size $L_T = 1$ m, and a receiving SIS (in blue) of size $L_R = 20$ cm, considering a generic orientation (same configuration of Fig. 5 corresponding to $N = 7$ communication modes.)

already considered in Fig. 5 are reported in Fig. 11 as example. In this case, despite the difference of size between the LIS and the SIS, the transmitting LIS can focus up to $N = 7$ beams in the SIS, and both antennas are within the respective boundary between near field and far field of the other one, when considering $m = 16$.

Regardless the condition for activating multiple communication modes, Sec. III-B has highlighted how, when one antenna is much larger than the other, the traditional relation (16) is not valid anymore, and a much more accurate expression is (38). This is reasonable, since the number of communication modes cannot grow to any possible value if the distance z is reduced or very large LISs are adopted. Differently, the two relations are equivalent when the distance is large, and in particular when $L_R \ll z$. By comparing (16) and (38), it is easy to show that, for example, at $z = L_R/2$ the actual number of communication modes is a half of that predicted by (16), while at $z = L_R/(2\sqrt{2})$ we have only one third of that. This condition depends on geometrical aspects only and it is not a function of the operating frequency.

Analyzing the expression for the number of communication modes valid in the near field here derived, it can be noticed that, in (38), the number of communication modes is not a function of L_R and z themselves, but of their ratio L_R/z . Specifically, it is possible to write (38) as

$$N = 1 + \frac{2L_T}{\lambda\sqrt{1+4F^2}} \quad (69)$$

with $F = z/L_R$. The same number of communication modes can be obtained by keeping such a ratio constant. This fact can be easily explained in the angular domain. In fact, we have $L_R/(2z) = \tan\varphi_{\max}$ according to Fig. 8. Since the LIS was supposed located in the far field of the SIS (hypothesis of small transmitting antenna), the angular pattern of the SIS would not change with z , so that the same number of angular beams can be intercepted by keeping the ratio F constant. As example, Fig. 12 reports the directions of the orthogonal beams φ_n of Fig. 8 for the same setting of Fig. 2 ($N = 19$) and two receiving antennas with $F = 1$, leading to the same number $N = 9$ of

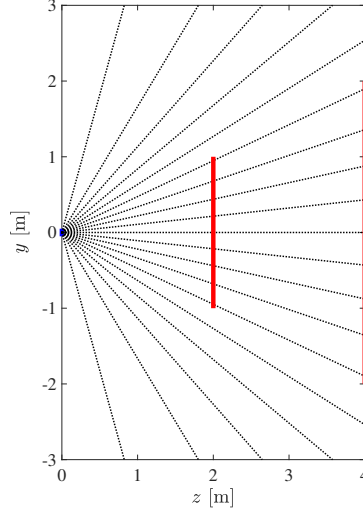


Fig. 12. Directions of the orthogonal beams for a SIS of size $L_T = 10$ cm (on the left at $y = 0$), in the same configuration of Fig. 2. Two LIS characterized with the same ratio $F = z/L_R = 1$ are shown (in red), highlighting that the same number $N = 9$ of communication modes can be realized (intercepted beams).

communication modes, as predicted by (69). Similarly, for perpendicular antennas, we have

$$N = 1 + \frac{L_T \left(\sqrt{1 + 4F^2} - 2F \right)}{\lambda \sqrt{1 + 4F^2}}. \quad (70)$$

Summarizing:

- 1) The operation in the near field is necessary condition to establish multiple communication modes; in particular, with operation in the near field should be intended the inclusion of at least one antenna in the near field of the other one. The design variables for exploiting this multi-mode communication are both the size of antennas and the operating frequency;
- 2) When the link distance becomes comparable with the size D of the largest antenna (e.g., $z < D$), ad-hoc models for evaluating the number of communication modes must be considered and traditional results, e.g., (16), fail.
- 3) For very large LISs or very small distance among the antennas, the number of communication modes depends mainly on the size of the smallest antenna only; in the general case, the number of communication modes is a function of the ratio $F = z/D$, where D is the size of the largest antenna.

The second condition has been found recently also for results related to the path loss involving LISs and/or large antenna arrays and has been defined as *geometric near field* [11], [12].

V. EXAMPLES

In this section, some numerical results are offered in order to discuss the proposed methods. Results are compared with numerical solutions obtained using SVD. In this case, the transmitting and receiving antenna are discretized into

a fine mesh, then the Green function is evaluated and its SVD decomposition computed, leading to the transmitting and receiving functions. The number of communication modes is obtained as the number of eigenvalues whose sum corresponds to the 99% of the overall coupling gain.

A. Number of Communication Modes

Figure 13 reports the number of communication modes for communication between a SIS and a LIS; results are obtained with the derived expressions (38) and (40), (or (69) and (70)). Two frequency ranges are considered, corresponding to millimeter-wave band ($f_0 = 28$ GHz) and terahertz band ($f_0 = 300$ GHz). The traditional result valid for large distance (16) is reported for comparison. It can be noticed that the actual number of communication modes diverges from that predicted by (16) when the size of the largest antenna becomes comparable with the link distance, thus entering the geometric near field ($F \approx 1$). In particular, for very short distance or very large LIS (small F), the limits $2L_R/\lambda$ and L_R/λ arise for parallel and perpendicular antennas, respectively. Differently, at large distance or with a small antenna (large F) a single mode is obtained, especially for the lower frequency. Notice that a large number of communication modes can be exploited when communicating with SIS and a LIS of size comparable with the link distance (e.g., 16 communication modes in the millimeter-wave band and 170 communication modes in the terahertz band), thus enabling potentially a large improvement of the channel capacity, even in LOS conditions. In Fig. 13, the markers report the number of eigenvalues obtained with the numerical SVD (i.e., significative eigenvalues). It is possible to appreciate the good agreement between the number of practically-orthogonal beams obtained for a specific antenna size and orientation, and the number of significative eigenvalues. This confirms that the proposed beampoint modeling, and then the related expressions derived, can be adopted as general design formulae capable of overcoming the limits of the traditional results related to far field and paraxial approximation without resorting to numerical evaluations and optimal basis functions which might lead to implementation issues.

When a generic orientation θ among the antennas is considered, the results derived for the number of communication modes (41) is reported in Fig. 14. A SIS of size $L_T = 20$ cm is considered and a frequency $f_0 = 60$ GHz. It is possible to notice that the number of communication modes is minimum when antennas are perpendicular (most unfavorable condition), while it is maximum when antennas are parallel (most favorable condition). On each curve, for a specific value of L_R , the left-hand limit corresponds to the value N given by (38); differently, the right-hand limit corresponds to the value N given by (40). With the increasing size of L_R the curves move towards the upper side of the graph (larger number of communication modes), until reaching the upper bound given by (42). When the size of the LIS becomes large, the limit $2L_T/\lambda$ arises for parallel antennas (left-hand limit for the upper bound curve) and the limit L_T/λ arises for perpendicular antennas (right-hand limit for the upper bound curve). Also in this case, it is possible to appreciate the good agreement between the number of beams obtained for a specific antenna size and orientation, and the number of eigenvalues obtained with the numerical SVD solution (square markers). Thus, the new derived expressions can be used for an immediate computation of the actual number of communication modes in general configurations beyond the traditional paraxial approximation.

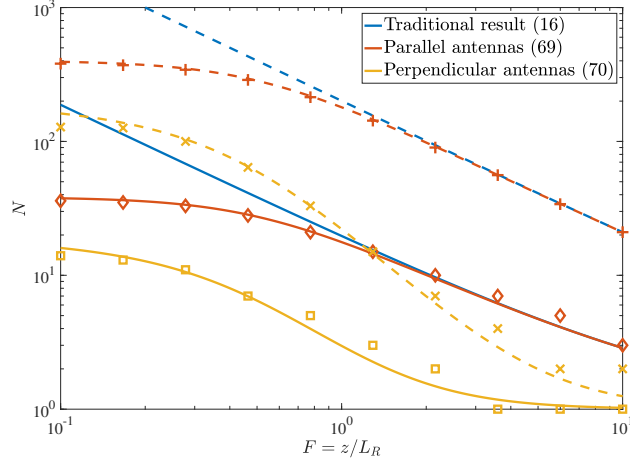


Fig. 13. Number of communication modes as a function of $F = z/L_R$ for parallel and perpendicular antennas, in comparison with traditional result (16). SIS of size $L_T = 20$ cm. Continuous lines (—) refer to the millimeter-wave band ($f_0 = 28$ GHz); dashed lines (--) refer to the terahertz band ($f_0 = 300$ GHz). Markers refer to the number of communication modes obtained with numerical solution (SVD).

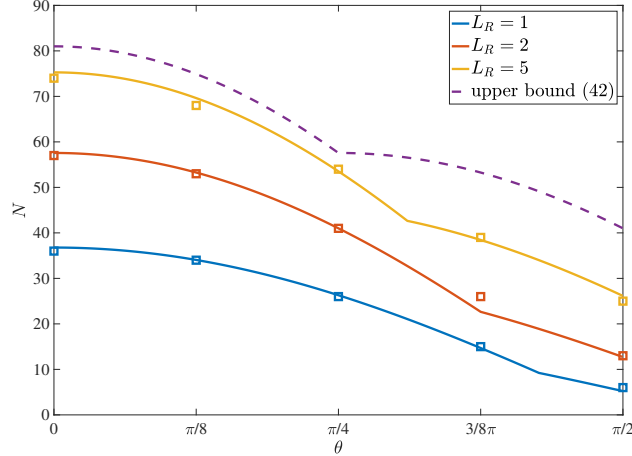


Fig. 14. Number of communication modes as a function of the orientation θ among the antennas for different size of the LIS, considering a SIS of size $L_T = 20$ cm, $z = 1$ m and $f_0 = 60$ GHz. Markers refer to the number of communication modes obtained with numerical solution (SVD).

B. TX/RX Basis Functions

In this section, the basis functions (hereinafter beams) obtained with the proposed method are compared with the functions at transmitting and receiving antenna side computed as SVD.

Table I compares the beams obtained considering a transmitting SIS and a receiving LIS (first row - uplink scenario) and beams obtained considering a transmitting LIS and a receiving SIS (second row - downlink scenario), constructed according to the method described in Sec. III-A. The two left-hand columns report the functions $\phi_n(\eta)$ and $\psi_n(y)$ (in amplitude and phase) at the SIS side of size 20 cm; the two right-hand columns report the functions $\psi_n(y)$ and $\phi_n(\eta)$ (in amplitude and phase) at the LIS side of size 1 m. As discussed, the transmitting side operates

phase-tapering only, so the amplitude function is not reported in this case (constant functions). In this table, a paraxial condition is considered, with $z = 5$ m. It is possible to see that the SIS uses a phase profile (i.e., functions $\phi_n(\eta)$) almost linear as expected (1b), corresponding to beam steering, and a small curvature can be noticed due to the relative short distance of the focal points on the receiving LIS, which is in the near-field of the SIS (corresponding to 7.5 m thus larger than z). In fact, $N = 3$ beams (functions $|\psi_n(y)|$ in 1c) are realized on the receiving antenna exploiting the proposed method.¹⁷ At the transmitting antenna side, the worst-case cross-correlation among the three functions $\phi_n(\eta)$ is -65 dB; at the receiving antenna side it is -25 dB, thus interesting for practical applications. When changing the role between transmitter and receiver (i.e., downlink), the transmitting LIS realizes focusing (functions $\phi_n(\eta)$ in 2d) and $N = 3$ beams (functions $|\psi_n(y)|$ in 2a) are realized on the receiving SIS (same number of the uplink, as expected). At the transmitting antenna side, the worst-case cross-correlation among the three functions $\phi_n(\eta)$ is -43 dB; at the receiving antenna side it is -25 dB. The third row of figures shows the exact solutions (optimal beams) obtained with SVD (3a-3d). In this case, the beams tend to occupy all the region of space of antennas, and the number of beams for each communication mode corresponds to the mode index. Moreover, it can be noticed that the same shape (in amplitude) is obtained at the SIS and LIS sides, despite the different size of the antennas. Both amplitude and phase tapering are exploited both at transmitting and receiving antenna side, and perfect orthogonality is realized.

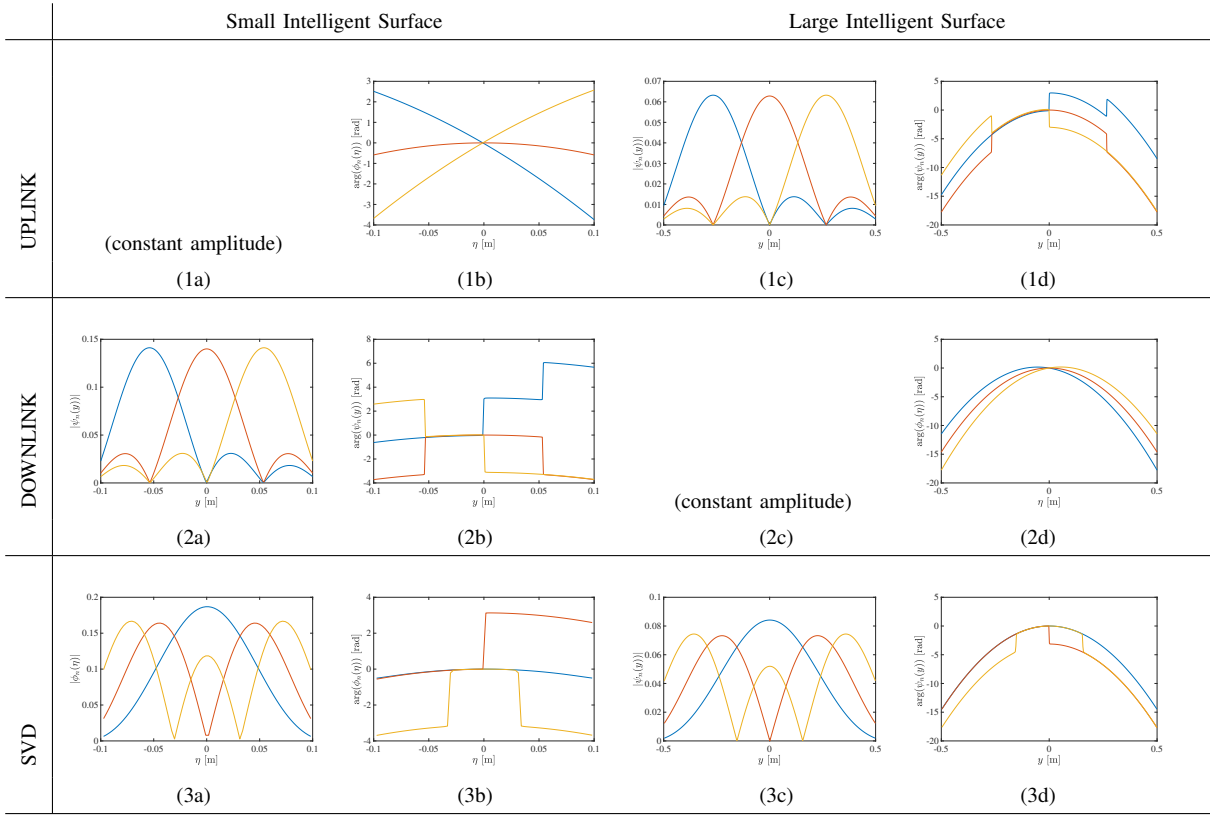
Then, Table II compares the beams obtained using the proposed method for uplink and downlink in a non-paraxial scenario. In particular, the same size of antennas of Table I are considered, but with an orientation $\theta = \pi/4$ and at $z = 2$ m. The two left-hand columns report the functions $\phi_n(\eta)$ and $\psi_n(y)$ (in amplitude and phase) at the SIS side of size 20 cm; the two right-hand columns report the functions $\psi_n(y)$ and $\phi_n(\eta)$ (in amplitude and phase) at the LIS side of size 1 m. In this case, it is possible to see that the $N = 6$ beams at the receiving antenna side (1c) are obtained using linear phase profiles at transmitting antenna side (1b). In fact, the receiving LIS is not located on the antenna boresight, resulting in a less pronounced focusing capability as discussed in Sec. IV. It is also evident the stretching of the lobe widths, which changes in the different parts of the LIS, resulting in a number of communication modes that cannot be predicted by traditional formulations related to paraxial approximation and small antennas, assuming intrinsically beams of constant width. At the transmitting antenna side the worst-case cross-correlation among the six functions $\phi_n(\eta)$ is -32 dB; at the receiving antenna side it is -25 dB. When changing the role between transmitter and receiver (i.e., downlink), the transmitting LIS realizes focusing (2d) and $N = 7$ beams (2a) are realized on the receiving SIS.¹⁸ At the transmitting antenna side the worst-case cross-correlation among the seven functions $\phi_n(\eta)$ is -21 dB; at the receiving antenna side it is -14 dB. The third row of figures shows the exact solutions obtained with SVD (3a-3d). Interestingly, in this case of non-paraxial scenario, the beams obtained on the LIS (3c) are similar to that realized with the proposed method, and they experience the same stretching of the widths.

¹⁷We can notice that, at the LIS side, a parabolic phase profile is obtained when beam steering is operated at the SIS side, which is not accounted by the analytic expression (35) and it is due to the first order approximation for both the phase profile at the SIS side and the Green function in (2).

¹⁸The number is slightly different from the $N = 6$ of the uplink due to the already-discussed border effects.

TABLE I

EXAMPLE OF TX/RX BASIS FUNCTIONS FOR UPLINK AND DOWNLINK, CONSIDERING A SIS OF 20 CM, A LIS OF 100 CM, $z = 5$ M, $\theta = 0$ (PARAXIAL CASE), $f_0 = 28$ GHZ. COMPARISON WITH OPTIMAL BASIS FUNCTIONS OBTAINED WITH SVD.



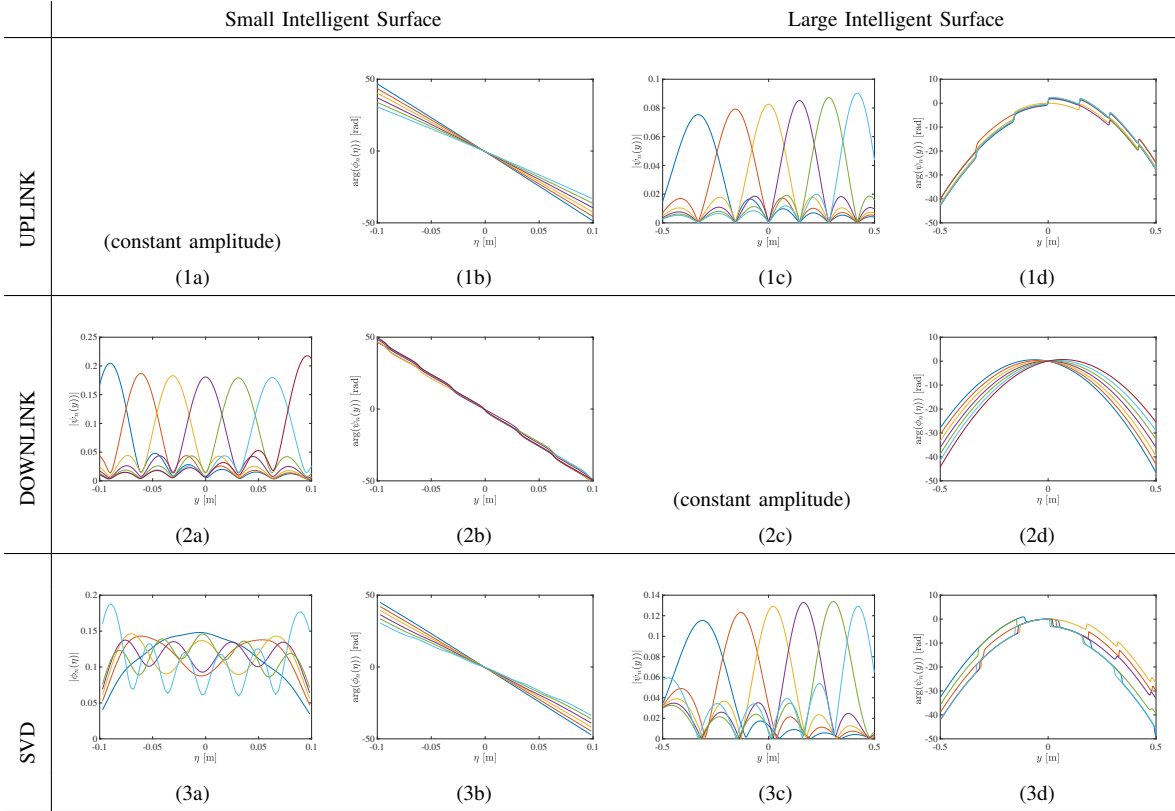
Although partially overlapped, every communication mode is characterized by a single beam on a specific point of the antenna, which is similar to the approach proposed.

VI. CONCLUSION

A simple and practical method for the definition of multiple communication modes in the near field has been proposed in this paper, exploiting concepts borrowed by diffraction theory and multi-focusing capability of large antennas. Starting from a beampspace modeling of communication modes, novel expressions for the number of modes have been derived, together with closed-form definitions for the basis set at the transmitting and receiving antennas for several cases of interest, such as the communication between a LIS and a SIS. It has been shown that almost-optimal basis sets can be designed starting from focusing functions, thus avoiding numerical evaluations and the implementation of complex amplitude/phase antenna profiles. The expressions derived for the number of communication modes are valid in a generic setup, beyond the traditional paraxial approximation, and account also for the intrinsic limits arising when the link distance becomes comparable to the antenna size (geometric near field). Traditional results valid under paraxial approximation have been revised in light of the proposed method, showing that the beampspace modeling leads to the same number of communication modes. The discussion on the operating

TABLE II

EXAMPLE OF TX/RX BASIS FUNCTIONS FOR UPLINK AND DOWNLINK CONSIDERING A SIS OF 20 CM, A LIS OF 100 CM, $z = 2$ M AND $\theta = \pi/4$ (NON-PARAXIAL CASE), $f_0 = 28$ GHZ. COMPARISON WITH OPTIMAL BASIS FUNCTIONS OBTAINED WITH SVD.



zones around a transmitting antenna, depending on the geometry and operating frequency conditions, has shown the relation among near-far field boundary definitions and the possibility of having multiple communication modes, thus enabling MIMO-like communication even in LOS channel conditions without exploiting multi-path propagation.

Future works will be targeted to the extension of the method here proposed in a generic 3D scenario, also including the complete description of the EM field as a vector, which could lead to additional degrees of freedom.

APPENDIX A

EVALUATION OF THE PHASE PROFILE IN THE UPLINK SCENARIO BETWEEN SIS AND LIS

We have

$$r(0) = \sqrt{z^2 + y^2} \quad (71)$$

and

$$\frac{\partial}{\partial \eta} r(\eta) = \frac{1}{2\sqrt{(z + \eta \sin \theta)^2 + (y - \eta \cos \theta)^2}} \left[\frac{\partial}{\partial \eta} (z + \eta \sin \theta)^2 + \frac{\partial}{\partial \eta} (y - \eta \cos \theta)^2 \right] \quad (72)$$

which gives

$$\frac{\partial}{\partial \eta} r(\eta) = \frac{(z + \eta \sin \theta) \sin \theta - (y - \eta \cos \theta) \cos \theta}{\sqrt{(z + \eta \sin \theta)^2 + (y - \eta \cos \theta)^2}}. \quad (73)$$

By posing $\eta = 0$ and discarding all the phase terms independent of η , since the addition of a constant phase shift would not change the focusing behavior, (25) is obtained.

APPENDIX B NUMBER OF COMMUNICATION MODES FOR PARALLEL ANTENNAS

We have

$$\frac{\lambda}{L_T} n^+ < \sin \arctan \frac{L_R}{2z}. \quad (74)$$

By exploiting $\sin \arctan(x) = x/\sqrt{1+x^2}$, it is obtained

$$n^+ < \frac{L_T L_R}{2\lambda z \sqrt{1 + \frac{L_R^2}{4z^2}}} \quad (75)$$

then (38).

APPENDIX C NUMBER OF COMMUNICATION MODES FOR PERPENDICULAR ANTENNAS

We have

$$\frac{\lambda}{L_T} n^+ - 1 < \sin \operatorname{arccot} \frac{L_R}{2z}. \quad (76)$$

By exploiting $\sin \operatorname{arccot}(x) = 1/\sqrt{1+x^2}$, it is obtained

$$n^+ < \frac{L_T}{\lambda} \left(1 - \frac{1}{\sqrt{1 + \frac{L_R^2}{4z^2}}} \right) \quad (77)$$

then (40).

APPENDIX D NUMBER OF COMMUNICATION MODES FOR THE GENERAL CASE

When considering a generic orientation θ and $y_c = 0$, the number of beams n^+ intercepted by the upper part of the receiving antenna will be different by the number of beams n^- intercepted by the lower half of the antenna.

Without loss of generality, let us consider $0 < \theta < \pi/2$.

A. Positive Semi-Axis

In this case we have $0 < y_n < L_R/2$, with $n < 0$. By inverting the relation

$$0 < z \tan \left[\arcsin \left(-\frac{\lambda}{L_T} k - \sin \theta \right) + \theta \right] < \frac{L_R}{2} \quad (78)$$

for $n = -1, -2, \dots - n^+$, it can be shown that

$$n^+ < \frac{L_T}{\lambda} \left[\sin \left(\arctan \frac{L_R}{2z} - \theta \right) + \sin \theta \right]. \quad (79)$$

Result (79) gives a number of beams increasing with θ up to $\theta = \frac{1}{2} \arctan \frac{L_R}{2z}$, then decreasing for larger values of θ . This is reasonable, since the number of communication modes related to beams in the positive semi-axis should first increase when the boresight direction of the transmitting antenna (where the emitted beams have a denser angular pattern) is oriented towards the positive semi-axis, then decrease for larger rotation values.

B. Negative Semi-Axis

In this case we have $-L_R/2 < y_n < 0$, with $n > 0$. Thus, by inverting the relation

$$-\frac{L_R}{2} < z \tan \left[\arcsin \left(-\frac{\lambda}{L_T} k - \sin \theta \right) + \theta \right] < 0 \quad (80)$$

for $n = 1, 2, \dots n^-$, it can be shown that

$$n^- < \frac{L_T}{\lambda} \left[\sin \left(\arctan \frac{L_R}{2z} + \theta \right) - \sin \theta \right]. \quad (81)$$

In order to have $n^- > 0$ from (81), it must be

$$\sin \left[\arctan \frac{L_R}{2z} - \theta \right] + \sin \theta > 0 \quad (82)$$

that results in

$$\theta < \frac{\pi}{2} - \frac{1}{2} \arctan \frac{L_R}{2z}. \quad (83)$$

C. Number of Communication Modes

For a generic θ with $0 \leq \theta \leq \pi/2$ we have

$$N = 1 + n^+ + n^- \quad (84)$$

where n^+ and n^- are given by (79) and (81), respectively.

REFERENCES

- [1] E. Björnson, L. Sanguinetti, H. Wymeersch, J. Hoydis, and T. L. Marzetta, “Massive MIMO is a reality - what is next?: Five promising research directions for antenna arrays,” *Digital Signal Processing*, 2019 (accessed December 01, 2020). [Online]. Available: <http://www.sciencedirect.com/science/article/pii/S1051200419300776>
- [2] C. De Lima, D. Belot, R. Berkvens, A. Bourdoux, D. Dardari, M. Guillaud, M. Isomursu, E.-S. Lohan, Y. Miao, A. N. Barreto, M. R. K. Aziz, J. Saloranta, T. Sanguanpuak, H. Sarieddeen, G. Seco-Granados, J. Suutala, T. Svensson, M. Valkama, B. Van Liempd, and H. Wymeersch, “Convergent communication, sensing and localization in 6G systems: An overview of technologies, opportunities and challenges,” *IEEE Access*, vol. 9, pp. 26 902–26 925, 2021.

- [3] S. Hu, F. Rusek, and O. Edfors, "Beyond massive MIMO: The potential of data transmission with large intelligent surfaces," *IEEE Trans. Signal Processing*, vol. 66, no. 10, pp. 2746–2758, May 2018.
- [4] S. A. Tretyakov, "Metasurfaces for general transformations of electromagnetic fields," *Philosophical Transactions of the Royal Society A: Mathematical, Physical and Engineering Sciences*, vol. 373, no. 2049, p. 20140362, 2015 (accessed December 01, 2020). [Online]. Available: <https://royalsocietypublishing.org/doi/abs/10.1098/rsta.2014.0362>
- [5] D. Gonzalez-Ovejero, G. Minatti, G. Chattopadhyay, and S. Maci, "Multibeam by metasurface antennas," *IEEE Trans. Antennas Propagat.*, vol. 65, no. 6, pp. 2923–2930, Feb. 2017.
- [6] C. L. Holloway, E. F. Kuester, J. A. Gordon, J. O'Hara, J. Booth, and D. R. Smith, "An overview of the theory and applications of metasurfaces: The two-dimensional equivalents of metamaterials," *IEEE Antennas and Propagation Magazine*, vol. 54, no. 2, pp. 10–35, April 2012.
- [7] N. Kaina, M. Dupré, G. Lerosey, and M. Fink, "Shaping complex microwave fields in reverberating media with binary tunable metasurfaces," *Scientific Reports*, vol. 4, no. 1, p. 6693, 2014. [Online]. Available: <https://doi.org/10.1038/srep06693>
- [8] Q. Wu, S. Zhang, B. Zheng, C. You, and R. Zhang, "Intelligent Reflecting Surface Aided Wireless Communications: A Tutorial," *arXiv e-prints*, p. arXiv:2007.02759, Jul. 2020.
- [9] M. D. Renzo, A. Zappone, M. Debbah, M. Alouini, C. Yuen, J. D. Rosny, and S. Tretyakov, "Smart radio environments empowered by reconfigurable intelligent surfaces: How it works, state of research, and road ahead," *IEEE J. Select. Areas Commun.*, vol. 38, no. 11, pp. 2450 – 2525, Jul. 2020.
- [10] D. Dardari and N. Decarli, "Holographic communication using intelligent surfaces," *IEEE Communications Magazine*, vol. 59, no. 6, pp. 35–41, 2021.
- [11] E. Björnson and L. Sanguinetti, "Power Scaling Laws and Near-Field Behaviors of Massive MIMO and Intelligent Reflecting Surfaces," *IEEE Open J. of the Communications Society*, vol. 1, pp. 1306 – 1324, Sep. 2020.
- [12] D. Dardari, "Communicating with large intelligent surfaces: Fundamental limits and models," *IEEE J. Select. Areas Commun.*, vol. 38, no. 11, pp. 2526–2537, Nov. 2020.
- [13] D. A. B. Miller, "Waves, modes, communications, and optics: a tutorial," *Adv. Opt. Photon.*, vol. 11, no. 3, pp. 679–825, Sep. 2019 (accessed December 01, 2020). [Online]. Available: <http://aop.osa.org/abstract.cfm?URI=aop-11-3-679>
- [14] ———, "Communicating with waves between volumes: evaluating orthogonal spatial channels and limits on coupling strengths," *Appl. Opt.*, vol. 39, no. 11, pp. 1681–1699, Apr. 2000. [Online]. Available: <http://ao.osa.org/abstract.cfm?URI=ao-39-11-1681>
- [15] J. Brady, N. Behdad, and A. M. Sayeed, "Beamspace MIMO for millimeter-wave communications: System architecture, modeling, analysis, and measurements," *IEEE Trans. Antennas Propagat.*, vol. 61, no. 7, pp. 3814–3827, 2013.
- [16] D. Headland, Y. Monnai, D. Abbott, C. Fumeaux, and W. Withayachumnankul, "Tutorial: Terahertz beamforming, from concepts to realizations," *APL Photonics*, vol. 3, no. 5, p. 051101, 2018.
- [17] Jeng-Shiann Jiang and M. A. Ingram, "Spherical-wave model for short-range MIMO," *IEEE Trans. Commun.*, vol. 53, no. 9, pp. 1534–1541, Sep. 2005.
- [18] F. Bohagen, P. Orten, and G. E. Oien, "On spherical vs. plane wave modeling of line-of-sight MIMO channels," *IEEE Trans. Commun.*, vol. 57, no. 3, pp. 841–849, Mar. 2009.
- [19] K. Nishimori, N. Honma, T. Seki, and K. Hiraga, "On the transmission method for short-range MIMO communication," *IEEE Trans. Veh. Technol.*, vol. 60, no. 3, pp. 1247–1251, Feb. 2011.
- [20] L. Hanlen and M. Fu, "Wireless communication systems with-spatial diversity: a volumetric model," *IEEE Trans. Wireless Commun.*, vol. 5, no. 1, pp. 133–142, Jan 2006.
- [21] R. Chen, W. X. Long, X. Wang, and L. Jiandong, "Multi-mode OAM radio waves: Generation, angle of arrival estimation and reception with UCAs," *IEEE Trans. Commun.*, vol. 19, no. 10, pp. 6932–6947, 2020.
- [22] T. Hu, Y. Wang, X. Liao, J. Zhang, and Q. Song, "OFDM-OAM modulation for future wireless communications," *IEEE Access*, vol. 7, pp. 59 114–59 125, 2019.
- [23] A. Trichili, K. Park, M. Zghal, B. S. Ooi, and M. Alouini, "Communicating using spatial mode multiplexing: Potentials, challenges, and perspectives," *IEEE Communications Surveys Tutorials*, vol. 21, no. 4, pp. 3175–3203, 2019.
- [24] K. Murata, N. Honma, K. Nishimori, N. Michishita, and H. Morishita, "Analog eigenmode transmission for short-range MIMO based on orbital angular momentum," *IEEE Trans. Antennas Propagat.*, vol. 65, no. 12, pp. 6687–6702, Aug. 2017.
- [25] R. Hansen, "Focal region characteristics of focused array antennas," *IEEE Trans. Antennas Propagat.*, vol. 33, no. 12, pp. 1328–1337, Dec. 1985.

- [26] P. Nepa and A. Buffi, "Near-field-focused microwave antennas: Near-field shaping and implementation." *IEEE Antennas Propagat. Mag.*, vol. 59, no. 3, pp. 42–53, Apr. 2017.
- [27] R. Liu and K. Wu, "Antenna array for amplitude and phase specified near-field multifocus," *IEEE Trans. Antennas Propagat.*, vol. 67, no. 5, pp. 3140–3150, Feb. 2019.
- [28] Z. H. Shaik, E. Bjrnson, and E. G. Larsson, "Cell-free massive MIMO with radio stripes and sequential uplink processing," in *2020 IEEE International Conference on Communications Workshops (ICC Workshops)*, 2020, pp. 1–6.
- [29] J. Goodman, *Introduction to Fourier Optics*, ser. Electrical Engineering Series. McGraw-Hill, 2005.
- [30] A. S. Y. Poon, R. W. Brodersen, and D. N. C. Tse, "Degrees of freedom in multiple-antenna channels: a signal space approach," *IEEE Trans. Inform. Theory*, vol. 51, no. 2, pp. 523–536, Feb 2005.
- [31] D. Slepian, "Some comments on Fourier analysis, uncertainty and modeling," *SIAM Review*, vol. 25, no. 3, pp. 379–393, 1983. [Online]. Available: <https://doi.org/10.1137/1025078>
- [32] C. Balanis, *Antenna Theory: Analysis and Design*. Wiley, 2015.
- [33] A. Sayeed and N. Behdad, "Continuous aperture phased MIMO: Basic theory and applications," in *2010 48th Annual Allerton Conference on Communication, Control, and Computing (Allerton)*, 2010, pp. 1196–1203.
- [34] F. Guidi and D. Dardari, "Radio positioning with EM processing of the spherical wavefront," *IEEE Trans. Wireless Commun.*, pp. 1–1, 2021, early access on-line.
- [35] A. Elzanaty, A. Guerra, F. Guidi, and M. Alouini, "Reconfigurable intelligent surfaces for localization: Position and orientation error bounds," *IEEE Trans. Signal Processing*, 2021, early access on-line.